INL/EXT-10-19969

Report on INL Activities for Uncertainty Reduction Analysis of FY10

G. Palmiotti
H. Hiruta
M. Salvatores
D. Fynan

September 2010

The INL is a U.S. Department of Energy National Laboratory
operated by Battelle Energy Alliance

INL/EXT-10-19969
FCRD-TRAN-2010-000152

Report on INL Activities for Uncertainty Reduction Analysis of FY10

G. Palmiotti
H. Hiruta
M. Salvatores
D. Fynan

September 2010

Idaho National Laboratory
Fuel Cycle Research & Development
Idaho Falls, Idaho 83415

http://www.inl.gov

Prepared for the
U.S. Department of Energy
Through the INL LDRD Program
Under DOE Idaho Operations Office
Contract DE-AC07-05ID14517

SUMMARY

The work scope of this project related to the Work Packages of "Uncertainty Reduction Analyses" with the goal of reducing nuclear data uncertainties is to produce a set of improved nuclear data to be used both for a wide range of validated advanced fast reactor design calculations, and for providing guidelines for further improvements of the ENDF/B files (i.e. ENDF/B-VII, and future releases).

This report presents the status of activities performed at INL under the FC R&D Work Package previously mentioned. First an analysis of uncertainty evaluation is presented using the new covariance data (AFCI version 1.2) made available by BNL. Then, analyses of a number of experiments, among those selected in the previous fiscal year and available, are presented making use of ENDF/B-VII data. These experiments include: updating of the ZPR-6/7 assembly (improved model and spectral indices), ZPPR-9 assembly (only simplified model available), ZPPR-10 (full detailed model), and irradiation experiments. These last experiments include PROFIL-1 were a new methodology has been employed in the Monte Carlo calculations, and also a deterministic analysis has been performed. This is the first time the Monte Carlo approach and ENDF/B-VII have been used for the PROFIL experiments. The PROFIL-2 and TRAPU experiments have been for the moment only modeled and a full analysis of the irradiation results will be finalized next fiscal year.

CONTENTS

TRANSMUTATION TECHNOLOGY/NUCLEAR DATA

1. INTRODUCTION

Recent extensive sensitivity/uncertainty studies, performed partly in the frame of AFCI (now FCR&D) and extensively supported within an international OECD-NEA initiative, have quantified for the first time the impact of current nuclear data uncertainties on design parameters of the major FCR&D and GEN-IV systems, and in particular on Na-cooled fast reactors with different fuels (oxide or metal), fuel composition (e.g. different Pu/TRU ratios) and different conversion ratios.

These studies have pointed out that present uncertainties on the nuclear data should be significantly reduced, in order to get full benefit from the advanced modeling and simulation initiatives.

Only a parallel effort in advanced simulation and in nuclear data improvement will enable to provide designers with more general and well validated calculation tools that would be able to meet design target accuracies.

The work scope of this project related to the Work Packages of "Uncertainty Reduction Analyses" with the goal of reducing nuclear data uncertainties is to produce a set of improved nuclear data to be used both for a wide range of validated advanced fast reactor design calculations, and for providing guidelines for further improvements of the ENDF/B files (i.e. ENDF/B-VII, and future releases).

This report presents the status of activities performed at INL under the FCR&D Work Package previously mentioned. First an analysis of uncertainty evaluation is presented using the new covariance data (AFCI version 1.2) made available by BNL. Then, analyses of a number of experiments, among those selected in the previous fiscal year and available, are presented making use of ENDF/B-VII data. These experiments include: updating of the ZPR-6/7 assembly (improved model and spectral indices), ZPPR-9 assembly (only simplified model available), ZPPR-10 (full detailed model), and irradiation experiments. These last experiments include PROFIL-1 were a new methodology has been employed in the Monte Carlo calculations, and also a deterministic analysis has been performed. The PROFIL-2 and TRAPU experiments have been for the moment only modeled and a full analysis of the irradiation results will be finalized next fiscal year.

2. UNCERTAINTY EVALUATION WITH AFCI 1.2 DATA

The first and most significant recent initiative aiming to a systematic nuclear data uncertainty impact assessment, was taken by the Working Party on Evaluation Cooperation (WPEC) of the OECD Nuclear Energy Agency Nuclear Science Committee when it established a Subgroup (called 26) to develop a systematic approach to define data needs for advanced reactor systems and to make a comprehensive study of such needs for Generation-IV (Gen-IV) reactors. The subgroup was established at the end of 2005, and a final report has been published in 2008 [1]. A comprehensive sensitivity and uncertainty study was performed to evaluate the impact of neutron cross-section uncertainty on the most significant integral parameters related to the core and fuel cycle of a wide range of innovative systems, even beyond the Gen-IV range of systems. In particular, results have been obtained for the Advanced Breeder Reactor (ABR), the Sodium-cooled Fast Reactor (SFR), the European Fast Reactor (EFR), the Gas-cooled Fast Reactor (GFR), the Lead-cooled Fast Reactor (LFR), and the Accelerator Driven Minor Actinide Burner (ADMAB). These systems correspond to current studies within the Generation-IV initiative, the Advanced Fuel Cycle Initiative (AFCI), and the advanced fuel cycle and Partitioning/Transmutation studies in Japan and Europe.

2.1 Sensitivity and uncertainty analysis

In order to perform the analysis, state-of-the-art sensitivity and uncertainty methods have been used based on the ERANOS code system [2].
The integral parameter uncertainties were initially calculated using covariance data developed in a joint effort of several laboratories contributing to the Subgroup activity. This set of covariance matrices was referred to as BOLNA [3].
The calculated integral parameter uncertainties, resulting from the initially assessed uncertainties on nuclear data of the BOLNA set, were found rather acceptable for the early phases of design feasibility studies. In fact, the uncertainty on keff was found to be less than 2% for all systems (with the exception of the Accelerator Driven System, ADS) and reactivity coefficient uncertainties below 20%. Power distributions uncertainties are also relatively small, except, once more, in the case of the ADS.
However, later conceptual and design optimization phases of selected reactor and fuel cycle concepts will need improved data and methods, in order to reduce margins, both for economical and safety reasons. For this purpose, a compilation of preliminary “Design Target Accuracies” has been put together and a target accuracy assessment has been performed to provide an indicative quantitative evaluation of nuclear data improvement requirements by isotope, nuclear reaction and energy range, in order to meet the Design target accuracies, as compiled in the present study. First priorities were formulated on the basis of common needs for fast reactors and, separately, thermal systems. These priority items (see Table I) have been included in the High Priority Request List (HPRL) of the OECD-NEA DataBank.

2.2 New covariance data for improved uncertainty analysis

Very recently, an effort lead by BNL [4] has produced an improved version of the initial covariance data (here called AFCI 1.2) with an energy group structure of 33 groups (instead of 15), and revised uncertainties have been calculated on the wide range of Fast Reactor systems considered above. The 15 group energy structure was intended to cover the entire energy spectrum so that a VHTR reactor and a high burn up PWR could be included in the Subgroup 26 study. The 33 group energy structure is devoted to specifically cover the fast reactor energy range. Typical results obtained with AFCI 1.2 and comparisons with previous data obtained with the BOLNA data are given in Tables II-XIII.
The overall uncertainties obtained with AFCI 1.2 confirm the order of magnitude of integral parameters uncertainties originally observed with BOLNA. The role of the uncertainty on U-238 inelastic cross

section is confirmed, as is the role of the Pu-241 fission cross section uncertainty, despite some significant variation between the uncertainties values in AFCI 1.2 with respect to BOLNA (see figure 1). In fact the Pu-241 fission uncertainty stays approximately the same between ~1MeV and ~1 keV and differs between the two covariance data libraries very strongly only above and below those energy values.

Table I. Summary of Highest Priority Target Accuracies for Fast Reactors from Subgroup 26

		Energy Range	Current (BOLNA) Accuracy (%)	Target Accuracy (%)
U238	σ_{inel}	6.07 ÷ 0.498 MeV	10 ÷ 20	2 ÷ 3
	σ_{capt}	24.8 ÷ 2.04 keV	3 ÷ 9	1.5 ÷ 2
Pu241	σ_{fiss}	1.35MeV ÷ 454 eV	8 ÷ 20	2 ÷ 3 (SFR,GFR,LFR) 5 ÷ 8 (ABTR, EFR)
Pu239	σ_{capt}	498 ÷ 2.04 keV	7 ÷ 15	4 ÷ 7
Pu240	σ_{fiss}	1.35 ÷ 0.498 MeV	6	1.5 ÷ 2
	ν	1.35 ÷ 0.498 MeV	4	1 ÷ 3
Pu242	σ_{fiss}	2.23 ÷ 0.498 MeV	19 ÷ 21	3 ÷ 5
Pu238	σ_{fiss}	1.35 ÷ 0.183 MeV	17	3 ÷ 5
Am242m	σ_{fiss}	1.35MeV ÷ 67.4keV	17	3 ÷ 4
Am241	σ_{fiss}	6.07 ÷ 2.23 MeV	12	3
Cm244	σ_{fiss}	1.35 ÷ 0.498 MeV	50	5
Cm245	σ_{fiss}	183 ÷ 67.4 keV	47	7
Fe56	σ_{inel}	2.23 ÷ 0.498 MeV	16 ÷ 25	3 ÷ 6
Na23	σ_{inel}	1.35 ÷ 0.498 MeV	28	4 ÷ 10
Pb206	σ_{inel}	2.23 ÷ 1.35 MeV	14	3
Pb207	σ_{inel}	1.35 ÷ 0.498 MeV	11	3
Si28	σ_{inel}	6.07 ÷ 1.35 MeV	14 ÷ 50	3 ÷ 6
	σ_{capt}	19.6 ÷ 6.07 MeV	53	6

Table II. ADMAB-EOC: keff Uncertainty (%) using AFCI 1.2

ISOTOPE	CAPTURE	ELASTIC	NU	INELASTIC	FISSION	SUM
PU238	0.04	0.00	0.14	0.03	1.29	1.29
CM245	0.01	0.00	0.12	0.01	1.12	1.13
CM244	0.64	0.00	0.56	0.07	0.72	1.12
AM241	0.60	0.00	0.30	0.19	0.83	1.08
PU241	0.08	0.00	0.03	0.01	0.95	0.95
CM242	0.05	0.00	0.08	0.03	0.68	0.68
AM243	0.30	0.00	0.09	0.24	0.40	0.56
NP237	0.18	0.00	0.06	0.18	0.35	0.44
BI209	0.06	0.05	0.00	0.30	0.00	0.31
PU240	0.13	0.00	0.16	0.02	0.15	0.26
AM242M	0.02	0.00	0.02	0.01	0.24	0.24
N15	0.01	0.22	0.00	0.01	0.00	0.22
PU242	0.07	0.00	0.04	0.03	0.19	0.21
PB206	0.02	0.01	0.00	0.19	0.00	0.19
PU239	0.08	0.01	0.07	0.08	0.11	0.18
SUM	0.98	0.24	0.70	0.55	2.42	2.77

Table III. ADMAB-EOC: keff Uncertainty Difference (%) between AFCI1.2 and BOLNA (major contributions)

ISOTOPE	CAPTURE	ELASTIC	NU	INELASTIC	FISSION	SUM
CM244	0.45	0.00	0.17	0.02	-1.38	-1.03
PU238	0.00	0.00	-0.18	0.02	0.79	0.70
FE56	0.05	-0.01	0.00	-0.69	0.00	-0.63
CM242	0.04	0.00	0.03	0.02	0.44	0.44
BI209	0.06	0.05	0.00	0.30	0.00	0.31
AM241	0.22	0.00	0.15	-0.05	0.11	0.22
N15	0.01	0.22	0.00	0.01	0.00	0.22
SUM	0.45	0.19	0.12	-0.39	-0.33	-0.24

Table IV. ABR-Metal-EOC: keff Uncertainty (%) using AFCI 1.2

ISOTOPE	CAPTURE	ELASTIC	NU	INELASTIC	FISSION	SUM
U238	0.18	0.17	0.14	0.97	0.04	1.01
PU241	0.07	0.00	0.02	0.00	0.66	0.67
PU238	0.02	0.00	0.06	0.01	0.56	0.56
PU240	0.29	0.01	0.30	0.02	0.27	0.50
PU239	0.16	0.03	0.12	0.08	0.20	0.30
PU242	0.09	0.00	0.04	0.02	0.19	0.21
CM245	0.00	0.00	0.02	0.00	0.21	0.21
FE56	0.15	0.12	0.00	0.03	0.00	0.20
NA23	0.00	0.07	0.00	0.08	0.00	0.11
CM244	0.07	0.00	0.05	0.00	0.06	0.11
AM241	0.05	0.00	0.02	0.01	0.04	0.07
CM242	0.01	0.00	0.01	0.00	0.06	0.06
FE54	0.05	0.03	0.00	0.01	0.00	0.06
AM242M	0.00	0.00	0.00	0.00	0.04	0.04
AM243	0.03	0.00	0.01	0.01	0.03	0.04
SUM	0.44	0.23	0.37	0.98	0.98	1.52

Table V. ABR-Metal-EOC: keff Uncertainty Difference (%) between AFCI1.2 and BOLNA (major contributions)

ISOTOPE	CAPTURE	ELASTIC	NU	INELASTIC	FISSION	SUM
PU238	0.00	0.00	-0.08	0.01	0.34	0.31
FE56	0.07	0.07	0.00	-0.28	0.00	-0.13
NA23	-0.02	0.03	0.00	-0.11	0.00	-0.09
SUM	0.03	0.03	-0.01	-0.03	0.16	0.09

Table VI. SFR: keff Uncertainty (%)

ISOTOPE	CAPTURE	ELASTIC	NU	INELASTIC	FISSION	TOTAL
PU238	0.06	0.00	0.16	0.02	1.31	1.32
PU241	0.13	0.00	0.03	0.01	0.99	1.00
PU240	0.47	0.01	0.44	0.03	0.39	0.76
AM242M	0.09	0.00	0.05	0.02	0.65	0.66
PU242	0.20	0.00	0.08	0.03	0.38	0.44
CM245	0.01	0.00	0.05	0.00	0.42	0.42
FE56	0.20	0.20	0.00	0.04	0.00	0.29
CM244	0.18	0.00	0.11	0.01	0.14	0.25
U238	0.05	0.04	0.03	0.23	0.01	0.24
PU239	0.13	0.02	0.08	0.06	0.13	0.21
AM241	0.10	0.00	0.04	0.01	0.09	0.14
NA23	0.01	0.02	0.00	0.11	0.00	0.11
CM242	0.01	0.00	0.01	0.00	0.11	0.11
AM243	0.06	0.00	0.01	0.02	0.06	0.09
FE54	0.07	0.05	0.00	0.01	0.00	0.08
TOTAL	0.64	0.21	0.51	0.27	1.91	2.11

Table VII. SFR: keff Uncertainty Difference (%) between AFCI1.2 and BOLNA (major contributions)

ISOTOPE	CAPTURE	ELASTIC	NU	INELASTIC	FISSION	TOTAL
PU238	0.00	0.00	-0.20	0.01	0.77	0.67
FE56	0.09	0.10	0.00	-0.41	0.00	-0.19
NA23	-0.01	0.01	0.00	-0.15	0.00	-0.15
CM244	0.12	0.00	0.03	0.00	-0.24	-0.15
B10	-0.14	-0.01	0.00	0.00	0.00	-0.14
PU240	0.16	0.00	0.01	0.02	0.03	0.11
TOTAL	0.18	0.10	-0.08	-0.29	0.37	0.30

Table VIII. EFR: keff Uncertainty (%)

ISOTOPE	CAPTURE	ELASTIC	NU	INELASTIC	FISSION	SUM
U238	0.25	0.16	0.13	0.89	0.03	0.95
PU240	0.33	0.00	0.28	0.02	0.26	0.51
PU241	0.05	0.00	0.01	0.00	0.40	0.40
PU239	0.25	0.02	0.15	0.08	0.20	0.37
PU238	0.02	0.00	0.04	0.01	0.34	0.34
PU242	0.06	0.00	0.02	0.01	0.08	0.11
NI58	0.10	0.00	0.00	0.02	0.00	0.11
FE56	0.10	0.02	0.00	0.02	0.00	0.10
O16	0.01	0.09	0.00	0.00	0.00	0.09
NA23	0.00	0.05	0.00	0.07	0.00	0.09
AM241	0.06	0.00	0.02	0.01	0.04	0.07
CM245	0.00	0.00	0.01	0.00	0.06	0.06
CM244	0.04	0.00	0.02	0.00	0.02	0.05
FE54	0.03	0.00	0.00	0.01	0.00	0.03
AM242M	0.00	0.00	0.00	0.00	0.03	0.03
SUM	0.52	0.20	0.35	0.90	0.63	1.28

Table IX. EFR: keff Uncertainty Difference (%) between AFCI1.2 and BOLNA (major contributions)

ISOTOPE	CAPTURE	ELASTIC	NU	INELASTIC	FISSION	SUM
PU238	0.00	0.00	-0.06	0.00	0.21	0.18
O16	-0.25	0.04	0.00	-0.03	0.00	-0.17
FE56	0.04	0.00	0.00	-0.16	0.00	-0.09
PU240	0.08	0.00	0.00	0.01	0.04	0.07
SUM	-0.06	0.01	0.01	0.00	0.10	0.02

Table X. GFR: keff Uncertainty (%)

ISOTOPE	CAPTURE	ELASTIC	NU	INELASTIC	FISSION	SUM
U238	0.29	0.14	0.16	1.50	0.04	1.54
PU241	0.08	0.00	0.03	0.01	0.80	0.80
PU238	0.03	0.00	0.06	0.01	0.54	0.54
AM241	0.26	0.00	0.09	0.03	0.26	0.38
PU240	0.20	0.00	0.20	0.02	0.21	0.36
PU239	0.22	0.01	0.13	0.07	0.15	0.30
PU242	0.15	0.00	0.05	0.03	0.22	0.27
SI28	0.11	0.08	0.00	0.04	0.00	0.14
CM245	0.00	0.00	0.02	0.00	0.13	0.13
CM244	0.08	0.00	0.04	0.00	0.05	0.10
CGRA	0.00	0.05	0.00	0.07	0.00	0.09
AM243	0.05	0.00	0.01	0.02	0.04	0.07
NP237	0.04	0.00	0.01	0.02	0.05	0.07
ZR92	0.03	0.04	0.00	0.01	0.00	0.05
ZR91	0.04	0.03	0.00	0.00	0.00	0.05
SUM	0.54	0.18	0.31	1.51	1.07	1.96

Table XI. GFR: keff Uncertainty Difference (%) between AFCI1.2 and BOLNA (major contributions)

ISOTOPE	CAPTURE	ELASTIC	NU	INELASTIC	FISSION	SUM
PU238	0.00	0.00	-0.09	0.01	0.33	0.29
CGRA	-0.01	-0.26	0.00	0.02	0.00	-0.23
SI28	0.11	0.08	0.00	0.04	0.00	0.14
SUM	-0.04	-0.16	-0.01	0.07	0.11	0.08

Table XII. LFR: keff Uncertainty (%)

ISOTOPE	CAPTURE	ELASTIC	NU	INELASTIC	FISSION	SUM
PU238	0.04	0.00	0.10	0.01	0.93	0.93
U238	0.17	0.08	0.10	0.81	0.03	0.84
PU240	0.40	0.00	0.38	0.06	0.32	0.64
PU241	0.07	0.00	0.02	0.01	0.61	0.61
PB206	0.08	0.03	0.00	0.33	0.00	0.34
PU239	0.17	0.01	0.12	0.11	0.20	0.31
PB208	0.10	0.22	0.00	0.06	0.00	0.25
CM245	0.00	0.00	0.02	0.00	0.23	0.23
PU242	0.10	0.00	0.04	0.02	0.18	0.21
PB207	0.09	0.03	0.00	0.10	0.00	0.14
FE56	0.11	0.05	0.00	0.02	0.00	0.12
AM241	0.08	0.00	0.02	0.02	0.06	0.11
CM244	0.07	0.00	0.04	0.01	0.05	0.09
AM242M	0.01	0.00	0.00	0.00	0.06	0.06
ZR92	0.04	0.03	0.00	0.03	0.00	0.06
SUM	0.54	0.25	0.43	0.90	1.21	1.68

Table XIII. LFR: keff Uncertainty Difference (%) between AFCI1.2 and BOLNA (major contributions)

ISOTOPE	CAPTURE	ELASTIC	NU	INELASTIC	FISSION	SUM
PU238	0.00	0.00	-0.13	0.01	0.58	0.52
B10	-0.27	-0.02	0.00	0.00	0.00	-0.27
PB206	-0.03	0.01	0.00	0.18	0.00	0.16
FE56	0.06	0.03	0.00	-0.22	0.00	-0.12
PB208	0.06	0.09	0.00	0.02	0.00	0.11
PU240	0.15	0.00	0.01	0.03	0.01	0.10
SUM	0.01	0.10	-0.03	0.04	0.37	0.28

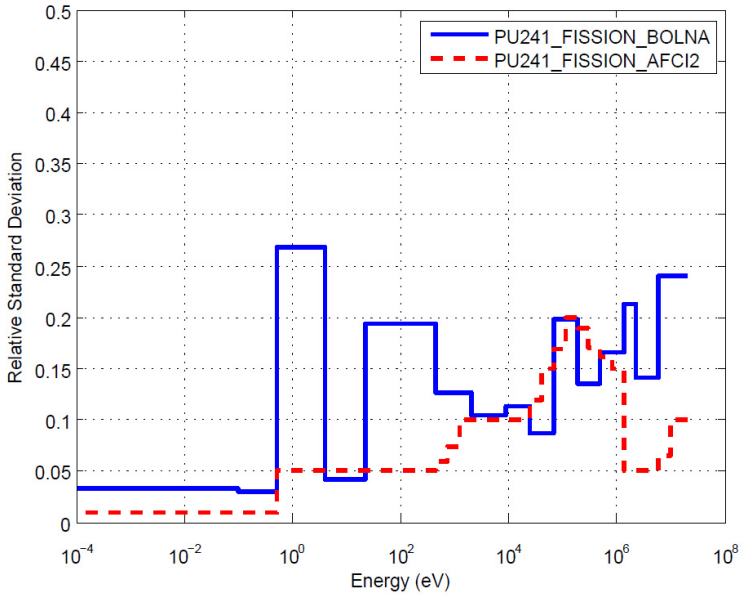

Figure 1. Relative Standard Deviation of Pu241 Fission Cross-sections in BOLNA and AFCI 1.2

The major contributions to the difference between the two covariance data sets are the Pu238 fission cross section uncertainty (much higher uncertainty values in AFCI 1.2, see figure 2) and the inelastic cross section of Fe56 (much smaller in AFCI 1.2, see Figure 3). These are certainly issues that need further analysis.

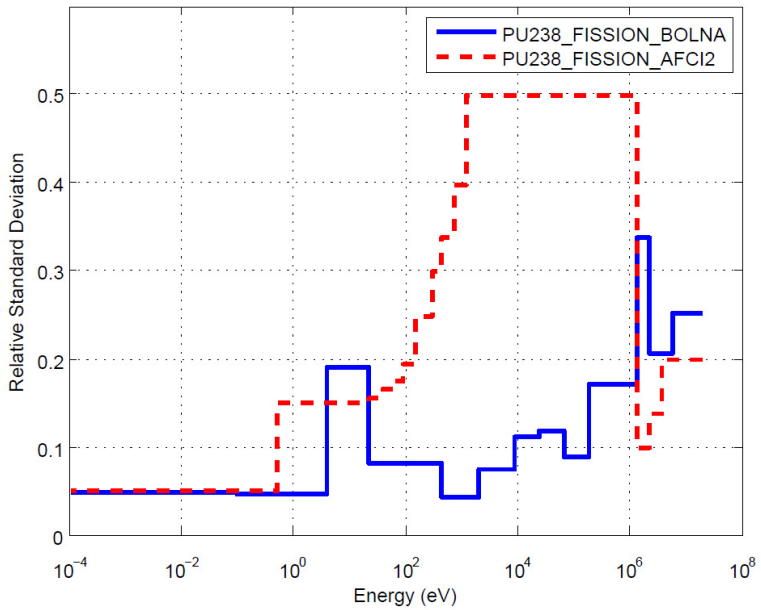

Figure 2. Relative Standard Deviation of Pu238 Fission Cross-sections in BOLNA and AFCI 1.2

The AFCI 1.2 uncertainty data for Pu238 are based on a comparative analysis done by Maslov, as indicated in Ref. 4. He compared evaluations in major data libraries and considered his own results and experimental data. Estimated uncertainties are based on difference with ENDF/B VII.0.

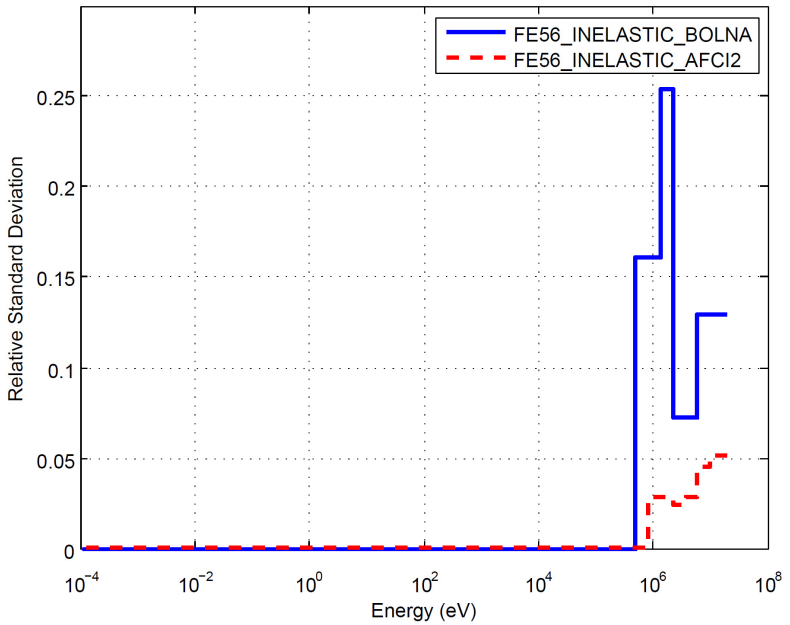

Figure 3. Relative Standard Deviation of Fe56 Inelastic Scattering Cross-sections in BOLNA and AFCI 1.2

As for minor actinides, their uncertainties continue to play an important role when the MA content in the core fuel is high (i.e. ADMAB and SFR). However, the AFCI 1.2 values confirm the previous analysis with BOLNA in the case of Cm245 (see Figure 4, where fission cross section uncertainties are compared)

and Am241, but give a lower uncertainty associated to the fission of Cm244 (see figure 5, relative to the fission cross section uncertainties in both covariance data sets).

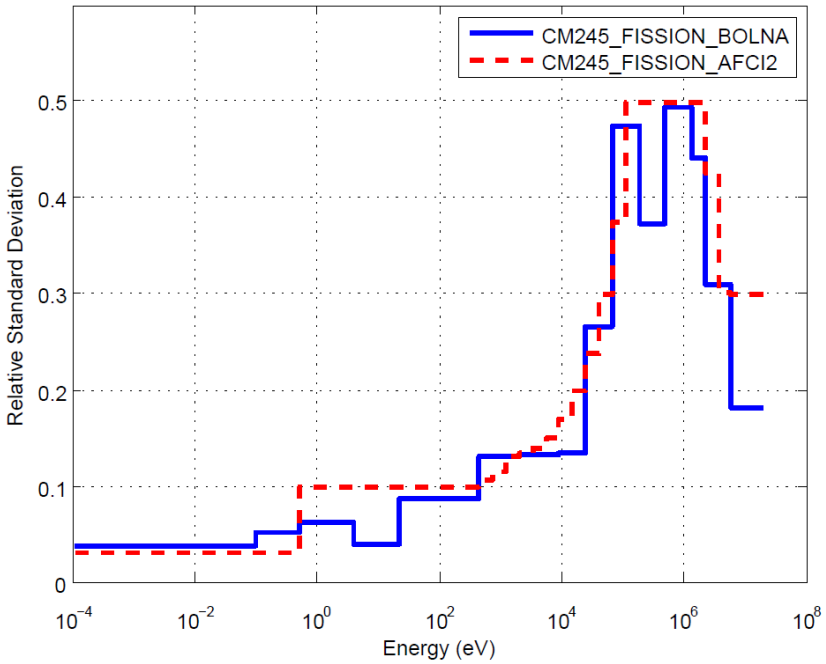

Figure 4. Relative Standard Deviation of Cm245 Fission Cross-sections in BOLNA and AFCI 1.2

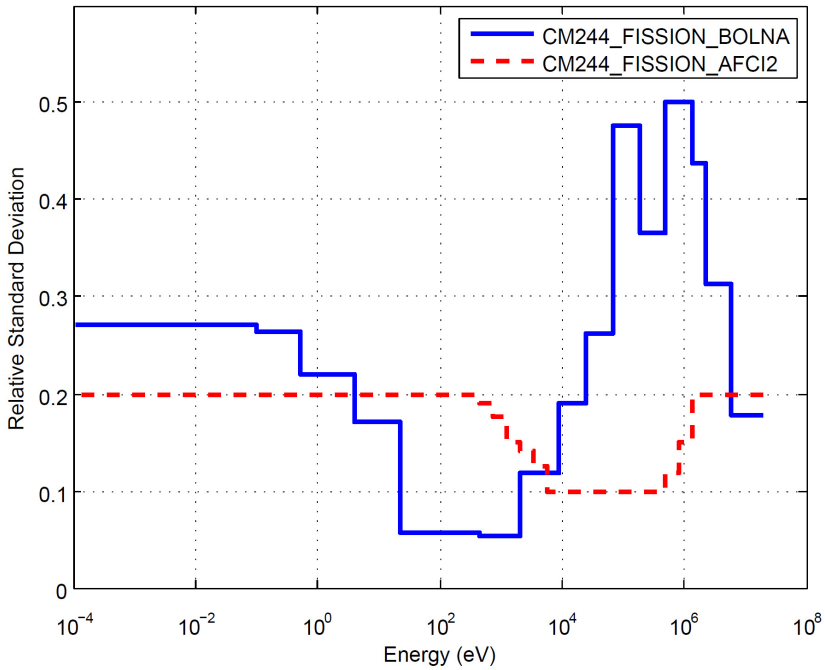

Figure 5. Relative Standard Deviation of Cm244 Fission Cross-sections in BOLNA and AFCI 1.2

Finally in the case of GFR it is interesting to point out the impact of the strong uncertainty reduction in AFCI 1.2 of the C elastic cross section (see figure 6 for the corresponding uncertainties comparison in

AFCI 1.2 and BOLNA). The AFCI 1.2 uncertainty values are a LANL estimate. In the energy range 1 keV – 1.8 MeV, the C elastic cross section is a standard, and the latest evaluation gives uncertainties in the range ~0.5-0.9%.

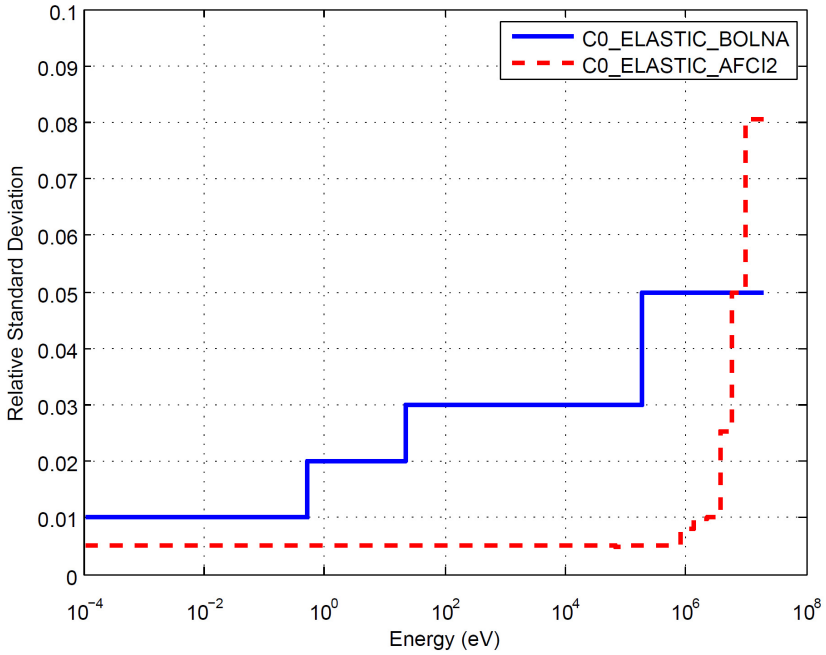

Figure 6. Relative Standard Deviation of C Elastic Scattering Cross-sections in BOLNA and AFCI 1.2

Table XIV. SFR: Coolant-voided Reactivity Uncertainty (%) by Isotope (Full AFCI 1.2 Correlation Data)

ISOTOPE	CAPTURE	ELASTIC	NU	INELASTIC	FISSION	SUM
PU238	0.67	0.04	0.36	0.17	8.78	8.82
NA23	0.35	1.02	0.00	4.82	0.00	4.94
FE56	1.43	4.46	0.00	0.39	0.00	4.70
PU241	0.59	0.04	0.14	0.20	3.98	4.04
PU240	1.27	0.11	2.46	0.49	2.46	3.74
PU242	2.37	0.04	0.60	0.20	2.20	3.29
AM242M	0.71	0.02	0.26	0.21	2.45	2.57
CM244	1.99	0.02	0.76	0.08	0.77	2.27
PU239	1.13	0.34	1.07	0.65	0.91	1.94
U238	0.76	0.60	0.10	1.57	0.02	1.85
CM245	0.05	0.00	0.26	0.03	1.05	1.09
AM241	0.78	0.02	0.19	0.20	0.44	0.94
FE54	0.33	0.85	0.00	0.06	0.00	0.91
AM243	0.64	0.02	0.05	0.26	0.25	0.74
NP237	0.64	0.01	0.05	0.20	0.24	0.72
SUM	4.27	4.81	2.91	5.20	10.63	13.78

As for the other parameters considered in the study of Subgroup 26 and reported in [1], the only significant new effect is related to the very high uncertainty of the Pu238 fission cross section in AFCI 1.2. In fact an uncertainty of ~9% is observed in the case of the Na void coefficient in the SFR system, see table XIV.
Finally, the new AFCI 1.2 covariance data set has some cross correlations between cross sections for a few isotopes and reactions (see Table XV). Their effect is very small at present. However, the generalization of this type of data in future versions of the covariance data sets will improve their quality and reliability.

Table XV. List of Isotopes with Cross-Reaction Correlations in AFCI 1.2

B10	ELASTIC x INELASTIC	GD155	ELASTIC x CAPTURE	U233	ELASTIC x N->2N
B10	INELASTIC x CAPTURE	GD157	ELASTIC x CAPTURE	U233	ELASTIC x FISSION
B11	ELASTIC x INELASTIC	GD160	ELASTIC x CAPTURE	U233	ELASTIC x CAPTURE
B11	ELASTIC x N->2N	H2	ELASTIC x N->2N	U233	FISSION x CAPTURE
B11	ELASTIC x CAPTURE	LI7	ELASTIC x INELASTIC	U235	ELASTIC x INELASTIC
BE9	ELASTIC x N->2N	MN55	ELASTIC x INELASTIC	U235	ELASTIC x N->2N
BE9	ELASTIC x CAPTURE	MN55	ELASTIC x N->2N	U235	ELASTIC x FISSION
C12	ELASTIC x INELASTIC	MN55	ELASTIC x CAPTURE	U235	ELASTIC x CAPTURE
C12	INELASTIC x CAPTURE	N15	ELASTIC x INELASTIC	U235	FISSION x CAPTURE
CM246	ELASTIC x INELASTIC	N15	ELASTIC x N->2N	U238	ELASTIC x INELASTIC
CM246	ELASTIC x N->2N	N15	ELASTIC x CAPTURE	U238	ELASTIC x N->2N
CM246	ELASTIC x FISSION	NA23	ELASTIC x CAPTURE	U238	ELASTIC x FISSION
CM246	ELASTIC x CAPTURE	NI58	ELASTIC x CAPTURE	U238	ELASTIC x CAPTURE
CR52	ELASTIC x CAPTURE	O16	ELASTIC x INELASTIC	U238	FISSION x CAPTURE
CR53	ELASTIC x CAPTURE	O16	INELASTIC x N->2N	ZR90	ELASTIC x INELASTIC
F19	ELASTIC x INELASTIC	O16	INELASTIC x CAPTURE	ZR90	ELASTIC x N->2N
F19	ELASTIC x N->2N	PU239	ELASTIC x INELASTIC	ZR90	ELASTIC x CAPTURE
F19	INELASTIC x N->2N	PU239	ELASTIC x N->2N		
F19	ELASTIC x CAPTURE	PU239	ELASTIC x FISSION		
FE56	ELASTIC x INELASTIC	PU239	ELASTIC x CAPTURE		
FE56	ELASTIC x N->2N	PU239	FISSION x CAPTURE		
FE56	INELASTIC x N->2N	TH232	ELASTIC x FISSION		
FE56	ELASTIC x CAPTURE	TH232	ELASTIC x CAPTURE		
FE56	INELASTIC x CAPTURE	TH232	FISSION x CAPTURE		
FE56	N->2N x CAPTURE	U233	ELASTIC x INELASTIC		

2.3 Summary on uncertainty evaluation

The results of the present investigation indicate that a careful analysis is still needed in order to define the most appropriate and effective strategy for data uncertainty reduction. It seems that, besides a further consolidation of the present covariance data libraries, a strategy of combined use of integral and differential measurements should be further pursued in order to meet future requirements. Efforts in this direction are underway (see e.g. Ref. 5), and a new Subgroup has been established by the WPEC of the

NEA-NSC in order to evaluate and compare different approaches in the field of the so-called "statistical data adjustment" or "data assimilation" methods. The program of this new Subgroup (called "33"), is to inter-compare the statistical data adjustments performed simultaneously in different laboratories, starting from the same set of integral data and different cross section data sets. As for covariance data, the proposed exercise will have a first phase when all participants will use the same covariance data and a second phase when different covariance data sets will be used. The objective of the exercise is to verify at what extent a convergence of the adjusted data sets will be obtained. This type of outcome will greatly improve the perception of reliability of the adjusted data sets, in particular with respect to their respective domain of applicability. Moreover, the impact of different covariance data will be evaluated and the significance of having a set of data consistent with the original cross section libraries will be assessed.

3. EXPERIMENTAL ANALYSIS

This section of the report presents the progress in the analysis of selected integral experiments using Monte Carlo code MCNP5 [6] and ERANOS code system [2] with ENDF/B-VII cross sections library.

3.1 ZPPR-10A Benchmark for Reactivity Effects

The ZPPR-10A was assembled as a part of the JUPITER-I series experiments in order to simulate the end-of-cycle configuration of 600MWe class of sodium-cooled MOX fueled FBR core. The ZPPR-10A core is a hexagonal shaped core consisting of a number of stainless steel drawers with small plates of depleted uranium, sodium (carbonate), iron oxide, depleted U3O8, stainless steel, and Pu-U-Mo alloy. The detailed reference core configuration is shown in Figure 1 [7].

The control rod worth was measured by replacing sodium plates filled in 3×3 arrays of drawers in several control rod positions (CRPs) with 50% B4C plates and 50% sodium plates and measuring the excess reactivity of the resulting configuration. The reference configuration for the sodium void worth measurements was constructed by replacing double column fuel (DCF) drawers in the reference critical configuration with single column fuel (SCF) drawers at 20 selected matrix positions in order to make it subcritical. Then, the sodium void worth was measured by creating voided zones in selected drawers.

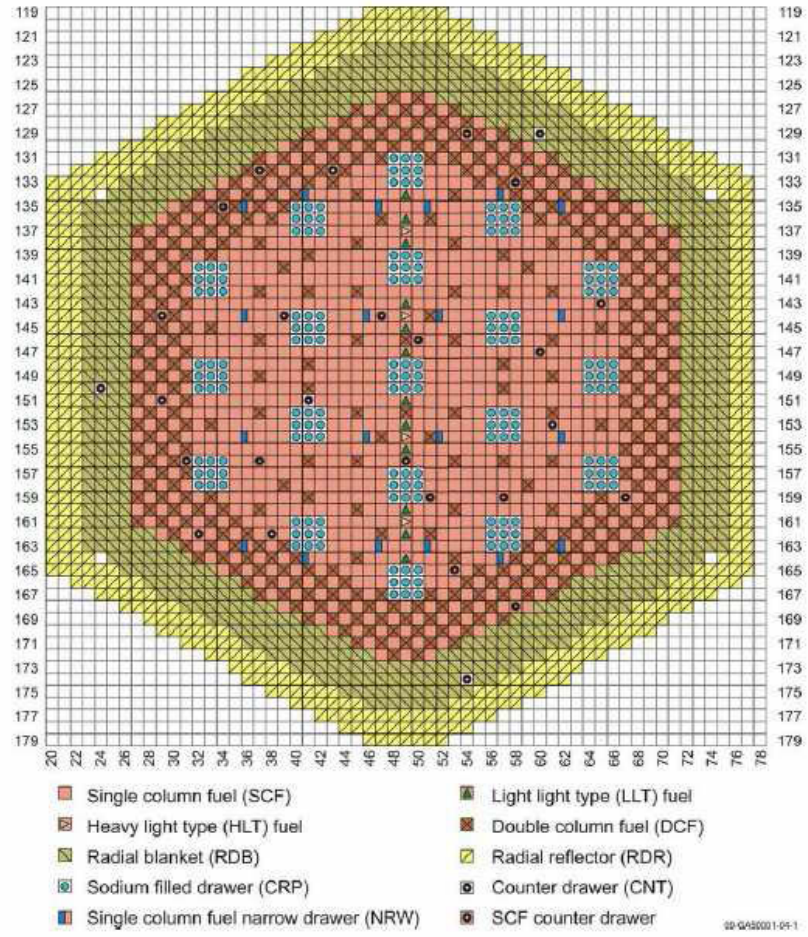

Figure 7: ZPPR-10A reference configuration (From Reference /2/).

MCNP calculations were performed for total of eight reactivity measurements (four for control rod worth and four for sodium void worth) using as-built models from IRPhEP document [7]. Based on k_{eff}'s obtained by MCNP calculations, the control rod worth were calculated by:

$$\Delta\rho_{CR} = \frac{k_{ref} - k_{rod}}{k_{ref} k_{rod} \beta_{eff}},$$

where k_{ref} is the neutron multiplication factor of the reference configuration, k_{rod} is that of the rodded configuration, and β_{eff} is the effective delayed neutron fraction, which was approximated by:

$$\beta_{eff} \cong \frac{k_{ref} - k_{prompt}}{k_{ref}},$$

where k_{prompt} is the multiplication factor calculated with only prompt neutrons. All multiplication factors here contain statistical errors. Thus, these statistical errors must be propagated into the error of control rod worth. This can be formulated as:

$$\sigma_{\Delta\rho_{CR}} = \sqrt{\left(\frac{1}{k_{ref}^2 \beta_{eff}}\right)^2 \sigma_{k_{ref}}^2 + \left(\frac{1}{k_{rod}^2 \beta_{eff}}\right)^2 \sigma_{k_{rod}}^2 + \left(\frac{1}{k_{ref} \beta_{eff}^2} - \frac{1}{k_{rod} \beta_{eff}^2}\right)^2 \sigma_{\beta_{eff}}^2},$$

where

$$\sigma_{\beta_{eff}} = \frac{k_{prompt}}{k_{ref}} \sqrt{\left(\frac{\sigma_{k_{prompt}}}{k_{prompt}}\right)^2 + \left(\frac{\sigma_{k_{ref}}}{k_{ref}}\right)^2}.$$

Similar formulations are used for sodium void reactivity calculations.
Tables XVI and XVII show experimental control rod worth and sodium void reactivity of each case, respectively, along with their C/E ratios based on our MCNP calculations. The calculated delayed neutron fraction is shown in the parenthesis at the bottom-left corner of each table. Comparisons were made with uncorrelated experimental values since the ZPPR-10A core was modeled explicitly. As seen in Tables, calculated control rod worth results have excellent agreement with experimental values, and results of all cases have similar quality of agreement. On the other hand, calculated values of sodium void reactivity have different quality of agreement. The magnitude of discrepancy becomes larger as the number of voiding zones becomes small. One of reasons could be due to the small order of reactivity (~50 cents) which requires much smaller statistical errors of k_{eff} from MC calculations than those for control rod worth calculations in order to obtain statistically reliable reactivity.

Table XVI: Comparison of ZPPR-10A Control Rod Worth

Radial Control Rod Position	Experiment [$] /2/	C/E
Central Control Rod	2.61 ± 0.03	1.0496 ± 0.0385
CR's 2-7, 6 rods in Ring 4	13.25 ± 0.14	1.0608 ± 0.0368
CR's 8-19, 12 rods in Ring 7	21.09 ± 0.31	1.0440 ± 0.0377
CR's 8, 10, 12, 14, 16, 18 in corners of Ring 7	9.54 ± 0.11	1.0501 ± 0.0368

(β_{eff} = 0.00343323 ± 0.00011305)

Table XVII: Comparison of ZPPR-10A Sodium Void Reactivity.

Voiding Zones	Experiment [cents] /2/	C/E
88 drawers, 8 inches per half	22.26 ± 0.26	1.2252 ± 0.0569
172 drawers, 8 inches per half	42.64 ± 0.46	1.0035 ± 0.0335
172 drawers, 16 inches per half	55.15 ± 0.61	1.0411 ± 0.0317
172 drawers, 20 inches per half	46.73 ± 0.52	0.9921 ± 0.0313

(β_{eff} = 0.00343315 ± 0.00004252)

3.2 ZPPR-9

The ZPPR-9 experiments were also conducted as a part of JUPITER program in order to provide integral reactor parameters for conventional mixed-oxide-fueled two-zone liquid metal fast breeder reactors (LMFBRs) of about 650 MWe. The ZPPR-9 assembly is a cylindrical core consisting of two clean homogeneous zones. There is no control-rod position. A simplified cylindrical model was developed for both MCNP and ERANOS deterministic calculations. A diagram of this model is shown in Figure 8.

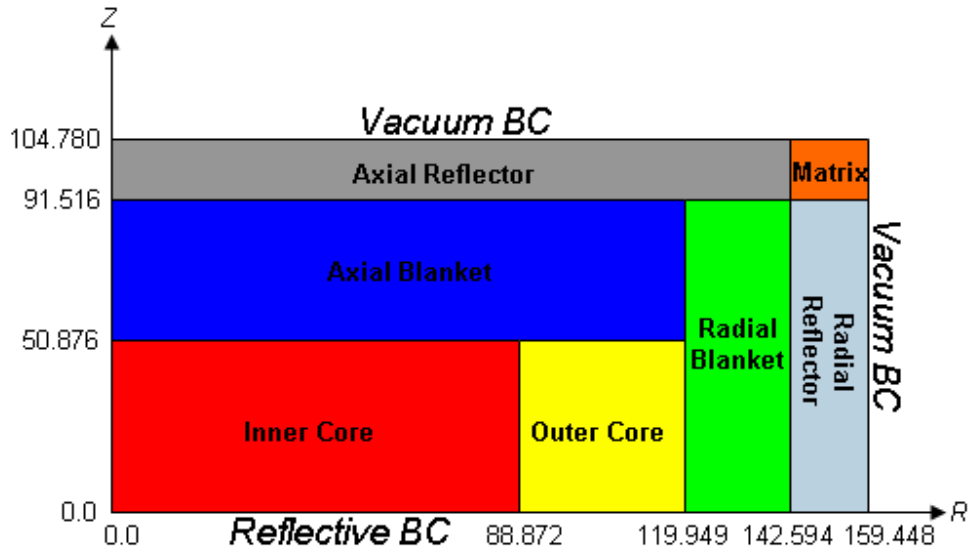

Figure 8: RZ Model of ZPPR-9 Core

Calculations of keff were performed using MC (MCNP) and SN (ERANOS) methods. For SN calculations, we utilized S4 quadratures with both P1 and P3 scattering expansions to see the possible effect of anisotropic scattering. Table XVIII shows the comparison of keff for ZPPR-9 models. The reference value shown here is the correlated value based on calculations performed by JAEA using JENDL library. Thus, it was expected to have some recognizable discrepancies from calculated values based on ENDF/B-VII. The difference between MCNP and ERANOS results is much smaller (less than 200 pcm) than the discrepancy from the reference value. In this respect, both models are consistent. There is a negligible effect caused by the difference in the order of scattering expansion. However, the effect can be significant when we analyze spectral indices at selected locations. The analysis of the spectral indices will be done in the next fiscal year.

Table XVIII: Comparison of k_{eff} for ZPPR-9 Models

	Reference	MCNP5	ERANOS (33-group, S4P1)	ERANOS (33-group, S4P3)
k_{eff}	0.99215 (±153 pcm)	0.98656 (±14 pcm)	0.98830	0.98840

3.3 ZPR6-7 Spectral indices

ZPR 6-7 is a large cylindrical assembly surrounded by a thick depleted-uranium reflector based on mixed Pu-U oxide fuels. There were two principal core configuration established for the ZPR6-7 program. Those were the uniform core loading and high ^{240}Pu-zone core loading [7]. The former had a relatively uniform core composition. A central zone of 61 matrix locations in each half of the assembly was defined as the exact core. This exact core region had the same unit cell and the same average composition as the outer core, but the plates used in the exact core were those for which knowledge of material properties was most precise. The latter configuration was a variant of the uniform core. The plutonium in the standard Pu-U-Mo fuel plates used in the uniform core contains 11% Pu240 . The high Pu240 zone was built by replacing all of the Pu-U-Mo plates in the exact core region of the uniform core with Pu-U-Mo plates containing 27% Pu240 in the plutonium component. The high Pu240 zone had a composition closer to that in an LMFBR core with high burnup [7].

In the last fiscal year, comparisons of k_{eff} and spectral indices were performed utilizing detailed geometry models. The comparison of k_{eff} had shown that the use of ENDF/B-VII did not contribute for reducing the discrepancy from the experimental result. This discrepancy was caused mainly due to the accuracy of our models. Therefore, we have decided to use detailed models from References 7 and 8. Table XIX shows the comparison of k_{eff} obtained with new and old models. As we see, results from new models were much closer to reference values than old ones.

Table XIX: Comparison of k_{eff} calculated with detailed ZPR6-7 models.

Assembly	Reference /2/	MCNP5 (old models)	MCNP5 (new models /2/)
Uniform core loading	1.00051±0.00087	0.99796±0.00007	1.00094±0.00007
High ^{240}Pu-zone core loading	1.0008±0.0009	0.99240±0.00007	1.00017±0.00011

The cell averaged spectral indices shown in the last year's report were calculated based on the volume weighted approach over each fuel plate at the central drawer (Figure 9). However, some of spectral indices showed large discrepancies (in particular, capture-to-fission ratio of U238). This indicated that the volume weighted approach was inappropriate. Therefore, we have utilized the atomic density weighted approach given by:

$$Reaction\ rate\ of\ Isotope\ n = \frac{\sum_{i=1}^{3} R_i^n A_i^n}{\sum_{i=1}^{3} A_i^n}$$

where R_i^n, and A_i^n refer to reaction rate and atomic density of Isotope n at Fuel plate i, respectively. Calculated results are compared in Table XX. More accurate solutions have been obtained by the atomic density weighted approach.

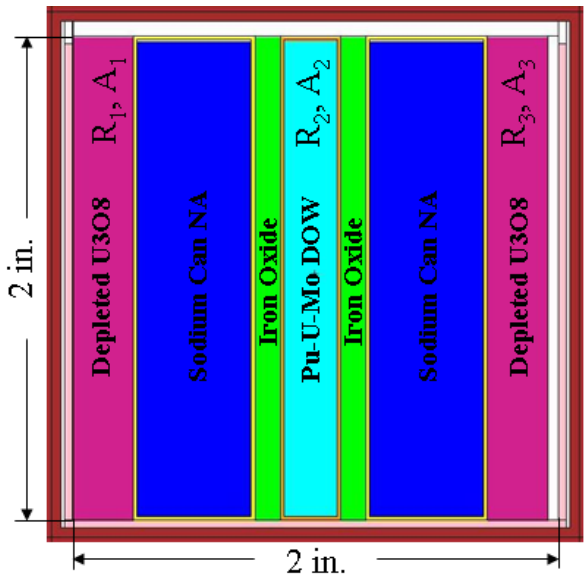

Figure 9: ZPPR6-7 central drawer.

Table XX: Comparison of spectral indices averaged over the central 2×2×2 inch box in ZPR6-7 core

Spectral Index	Experiment	C/E (Volume weighted)	C/E (Atomic density weighted)
$\sigma_f(^{235}U)/\ \sigma_f(^{239}Pu)$	1.0599 ± 0.0223	1.0317 ± 0.0224	1.0376 ± 0.0227
$\sigma_f(^{238}U)/\ \sigma_f(^{235}U)$	0.0223 ± 0.0007	0.9148 ± 0.0301	1.0045 ± 0.0328
$\sigma_f(^{238}U)/\ \sigma_f(^{239}Pu)$	0.0233 ± 0.0007	0.9571 ± 0.0300	1.0601 ± 0.0344
$\sigma_{n,\gamma}(^{238}U)/\ \sigma_f(^{235}U)$	0.1323 ± 0.0032	1.0227 ± 0.0257	1.0098 ± 0.0252
$\sigma_{n,\gamma}(^{238}U)/\ \sigma_f(^{239}Pu)$	0.1399 ± 0.0032	1.0572 ± 0.0252	1.0500 ± 0.0251
$\sigma_{n,\gamma}(^{238}U)/\ \sigma_f(^{238}U)$	5.8903 ± 0.1897	1.1243 ± 0.0381	1.0111 ± 0.0342

3.4 PROFIL-1 Analysis

The PROFIL-1 irradiation experiment was performed in the Phoenix reactor. The experiment provides a powerful source of information for the nuclear data adjustment for major and minor actinides and several fission products. In FY2009, the accuracy of PROFIL-1 model was validated by comparing initial k_{eff} and axial flux distribution to their experimental values. In order to perform three-dimensional burn-up Monte Carlo calculations, it is important to obtain accurate and statistically reliable one-group cross sections for each irradiated sample that are to be used for solving Bateman equations. However, it is extremely difficult to obtain statistically reliable tally results since the size of each sample is very small (~0.06 cm^3), and some of reactions (e.g., (n,2n), (n,3n)) are caused by very fast neutrons (5 MeV ~) which

are usually not well populated. Moreover, it is not straightforward to perform variance reduction in criticality calculations. Thus, we came up with a calculation procedure that uses MCNP's surface source capability (Figure 10). In this approach, first, a full-core criticality calculation is performed with the surface source write (SSW) card in order to generate the binary source file containing the surface and fission volume sources around and in the irradiated fuel samples, respectively. This source file is used to perform the fixed source calculation with the reduced geometry modeling only the irradiated fuel pin. The fixed source calculation can be performed with only the recorded particles from the full-core criticality calculation. If the number of recorded source particles is small, then it is not feasible to obtain statistically reliable solutions even with variance reduction techniques. In order to resolve this problem, we wrote a program that duplicates the recorded information of source particles. However, the number of duplications is limited because adding additional source particles enlarges the size of the source file. To address this issue, we performed several fixed source calculations by skipping random numbers corresponding to the number of histories for each run. After finishing all fixed source calculations, the solutions were collected, and then the batch statistics was taken.

Tables XXI-XXXIII show the calculated one-group cross sections for selected samples by this presented procedure.

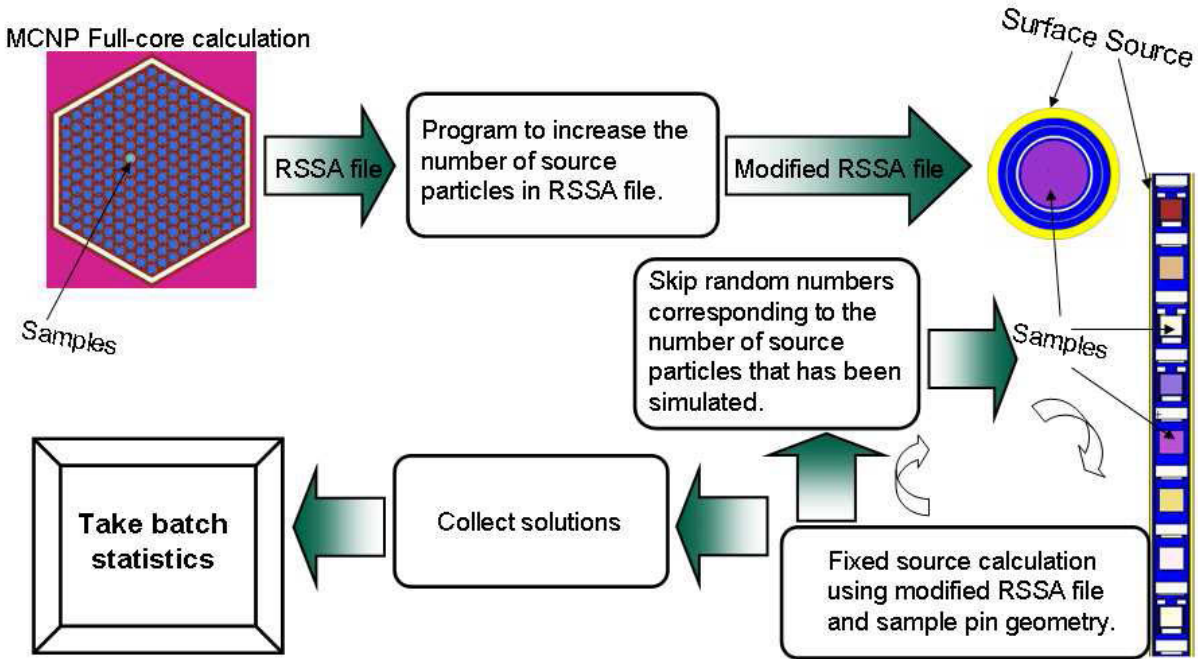

Figure 10: Procedure for calculating one-group cross sections by MCNP.

Table XXI: Calculated one-group cross sections for Sample 1 (U235)

Reaction (MT)[a]	Isotope	XS [barn]	Relative Error [%]	Reaction	Isotope	XS [barn]	Relative Error [%]
102	U234	4.552470E-01	0.576687	102	Nd143	2.462160E-01	1.187224
16	U234	3.037840E-04	5.405779	16	Nd143	1.060680E-03	4.712392
17	U234	2.042630E-07	41.586665	107	Nd143	1.372840E-04	0.497082
18	U234	3.515110E-01	0.340001	103	Nd143	1.397710E-06	9.41343
102	U235	5.200940E-01	0.28465	102	Nd144	6.744250E-02	1.061523
16	U235	1.615260E-03	2.973529	16	Nd144	5.659250E-04	7.274614
17	U235	1.654130E-06	39.896221	107	Nd144	5.179420E-06	1.374367
18	U235	1.843810E+00	0.231388	103	Nd144	5.070580E-07	21.592868
102	U236	4.178900E-01	0.5135	102	Nd145	4.136860E-01	1.015527
16	U236	9.402970E-04	4.394599	16	Nd145	1.780370E-03	4.104082
17	U236	5.890100E-06	38.603775	107	Nd145	2.559820E-05	0.291464
18	U236	1.152540E-01	0.455458	103	Nd145	4.080940E-07	17.544697
102	U238	2.748800E-01	0.486127	102	Nd146	8.008490E-02	0.890986
16	U238	2.170750E-03	3.776873	16	Nd146	7.393660E-04	6.734951
17	U238	1.432320E-05	37.1957	107	Nd146	8.312730E-07	5.250858
18	U238	5.018800E-02	0.573286	103	Nd146	1.401420E-07	32.150775
102	Np237	1.516370E+00	0.271159	102	Nd148	1.191480E-01	1.374542
16	Np237	4.541470E-04	4.254421	16	Nd148	9.196060E-04	5.955908
17	Np237	5.465450E-07	39.542921	107	Nd148	1.393440E-07	15.38162
18	Np237	3.748080E-01	0.352052	103	Nd148	5.878040E-08	35.712273
102	Pu239	4.613240E-01	0.501309	102	Nd150	1.307540E-01	1.702744
16	Pu239	4.858250E-04	3.357739	16	Nd150	8.367720E-04	6.161138
17	Pu239	8.652000E-07	41.354102	107	Nd150	3.463640E-08	29.090079
18	Pu239	1.783370E+00	0.241661	103	Nd150	2.584370E-08	38.230922

Table XXII: Calculated one-group cross sections for Sample 9 (Pu239)

Reaction (MT)	Isotope	XS [barn]	Relative Error [%]	Reaction	Isotope	XS [barn]	Relative Error [%]
102	U235	5.277180E-01	0.275358	17	Pu242	3.843550E-07	43.481297
16	U235	1.309630E-03	3.018402	18	Pu242	2.895290E-01	0.34421
17	U235	5.529250E-09	45.193093	102	Nd143	2.465200E-01	1.241947
18	U235	1.854340E+00	0.218769	16	Nd143	7.810170E-04	5.097732
102	U238	2.788660E-01	0.539614	107	Nd143	1.373350E-04	0.467075
16	U238	1.607300E-03	4.038454	103	Nd143	9.754650E-07	5.519241
17	U238	1.048170E-06	37.509085	102	Nd144	6.890200E-02	1.025881
18	U238	4.957540E-02	0.533836	16	Nd144	4.176980E-04	8.055213
102	Np237	1.530440E+00	0.255034	107	Nd144	4.775180E-06	1.017322
16	Np237	3.327800E-04	4.672836	103	Nd144	2.373220E-07	10.316824
17	Np237	1.248490E-09	44.918811	102	Nd145	4.119220E-01	0.827633
18	Np237	3.698680E-01	0.328834	16	Nd145	1.318890E-03	4.358531
102	Pu239	4.600080E-01	0.38868	107	Nd145	2.533040E-05	0.254283
16	Pu239	3.866480E-04	3.433756	103	Nd145	2.239480E-07	9.050768
17	Pu239	1.274760E-10	44.981367	102	Nd146	8.211380E-02	0.999629
18	Pu239	1.780460E+00	0.216757	16	Nd146	5.369370E-04	7.516264
102	Pu240	4.881350E-01	0.676284	107	Nd146	6.763460E-07	2.269745
16	Pu240	2.424250E-04	5.49969	103	Nd146	3.364360E-08	15.324273
17	Pu240	2.043910E-08	45.354636	102	Nd148	1.187430E-01	1.533633
18	Pu240	4.119750E-01	0.308059	16	Nd148	6.518660E-04	6.734455
102	Pu241	4.161960E-01	0.268581	107	Nd148	8.413170E-08	5.653535
16	Pu241	2.358720E-03	2.532586	103	Nd148	7.999490E-09	17.714538
17	Pu241	7.121060E-07	38.645888	102	Nd150	1.322880E-01	1.610215
18	Pu241	2.442180E+00	0.218104	16	Nd150	5.997310E-04	6.953367
102	Pu242	4.086690E-01	0.374421	107	Nd150	9.991550E-09	11.565467
16	Pu242	6.603680E-04	4.598729	103	Nd150	1.853950E-09	22.743318

[a] MT=16 : (n,2n), MT=17 : (n,3n), MT=18 : (n,f), MT=102 : (n,γ), MT=103 : (n,p), MT=107 : (n,α)

Table XXIII: Calculated one-group cross sections for Sample 12 (U238)

Reaction (MT)	Isotope	XS [barn]	Relative Error [%]	Reaction	Isotope	XS [barn]	Relative Error [%]
102	U235	5.277180E-01	0.275358	17	Pu242	3.843550E-07	43.481297
16	U235	1.309630E-03	3.018402	18	Pu242	2.895290E-01	0.34421
17	U235	5.529250E-09	45.193093	102	Nd143	2.465200E-01	1.241947
18	U235	1.854340E+00	0.218769	16	Nd143	7.810170E-04	5.097732
102	U238	2.788660E-01	0.539614	107	Nd143	1.373350E-04	0.467075
16	U238	1.607300E-03	4.038454	103	Nd143	9.754650E-07	5.519241
17	U238	1.048170E-06	37.509085	102	Nd144	6.890200E-02	1.025881
18	U238	4.957540E-02	0.533836	16	Nd144	4.176980E-04	8.055213
102	Np237	1.530440E+00	0.255034	107	Nd144	4.775180E-06	1.017322
16	Np237	3.327800E-04	4.672836	103	Nd144	2.373220E-07	10.316824
17	Np237	1.248490E-09	44.918811	102	Nd145	4.119220E-01	0.827633
18	Np237	3.698680E-01	0.328834	16	Nd145	1.318890E-03	4.358531
102	Pu239	4.600080E-01	0.38868	107	Nd145	2.533040E-05	0.254283
16	Pu239	3.866480E-04	3.433756	103	Nd145	2.239480E-07	9.050768
17	Pu239	1.274760E-10	44.981367	102	Nd146	8.211380E-02	0.999629
18	Pu239	1.780460E+00	0.216757	16	Nd146	5.369370E-04	7.516264
102	Pu240	4.881350E-01	0.676284	107	Nd146	6.763460E-07	2.269745
16	Pu240	2.424250E-04	5.49969	103	Nd146	3.364360E-08	15.324273
17	Pu240	2.043910E-08	45.354636	102	Nd148	1.187430E-01	1.533633
18	Pu240	4.119750E-01	0.308059	16	Nd148	6.518660E-04	6.734455
102	Pu241	4.161960E-01	0.268581	107	Nd148	8.413170E-08	5.653535
16	Pu241	2.358720E-03	2.532586	103	Nd148	7.999490E-09	17.714538
17	Pu241	7.121060E-07	38.645888	102	Nd150	1.322880E-01	1.610215
18	Pu241	2.442180E+00	0.218104	16	Nd150	5.997310E-04	6.953367
102	Pu242	4.086690E-01	0.374421	107	Nd150	9.991550E-09	11.565467
16	Pu242	6.603680E-04	4.598729	103	Nd150	1.853950E-09	22.743318

Table XXIV: Calculated one-group cross sections for Sample 13 (Pu240)

Reaction (MT)	Isotope	XS [barn]	Relative Error [%]	Reaction	Isotope	XS [barn]	Relative Error [%]
102	Pu238	6.976630E-01	0.362389	107	Nd143	1.384180E-04	0.473173
16	Pu238	5.935060E-04	5.380859	103	Nd143	1.429740E-06	7.894064
17	Pu238	2.937740E-05	25.009649	102	Nd144	7.023810E-02	1.316051
18	Pu238	1.155630E+00	0.227027	16	Nd144	5.513400E-04	6.39402
102	Pu239	4.576890E-01	0.407591	107	Nd144	5.062760E-06	1.216924
16	Pu239	4.369230E-04	3.224929	103	Nd144	5.967070E-07	16.238455
17	Pu239	1.341780E-06	28.588982	102	Nd145	4.067260E-01	0.858495
18	Pu239	1.781640E+00	0.216085	16	Nd145	1.627560E-03	3.941579
102	Pu240	4.784400E-01	0.500252	107	Nd145	2.554790E-05	0.26624
16	Pu240	3.199300E-04	4.633435	103	Nd145	4.571300E-07	13.747319
17	Pu240	1.832170E-06	25.359156	102	Nd146	7.985380E-02	0.756263
18	Pu240	4.168140E-01	0.304106	16	Nd146	7.273530E-04	5.936211
102	Pu241	4.176530E-01	0.365439	107	Nd146	8.347250E-07	4.544443
16	Pu241	2.489380E-03	2.396945	103	Nd146	1.909500E-07	21.552215
17	Pu241	5.433490E-06	22.437151	102	Nd148	1.234790E-01	1.541685
18	Pu241	2.437120E+00	0.218769	16	Nd148	8.961500E-04	5.385374
102	Pu242	4.118030E-01	0.434057	107	Nd148	1.557470E-07	12.126587
16	Pu242	8.176650E-04	4.123042	103	Nd148	7.992250E-08	22.947718
17	Pu242	1.451630E-05	22.949458	102	Nd150	1.307370E-01	1.43651
18	Pu242	2.942560E-01	0.342594	16	Nd150	8.137710E-04	5.533831
102	Nd143	2.571690E-01	1.510225	107	Nd150	4.531070E-08	20.221757
16	Nd143	9.772800E-04	4.444862	103	Nd150	3.866530E-08	25.071854

Table XXV: Calculated one-group cross sections for Sample 15 (Pu242)

Reaction (MT)	Isotope	XS [barn]	Relative Error [%]	Reaction	Isotope	XS [barn]	Relative Error [%]
102	Np237	1.517050E+00	0.252293	102	Cm242	3.103920E-01	0.710087
16	Np237	3.439560E-04	4.355573	16	Cm242	1.873460E-05	5.060783
17	Np237	1.418620E-07	31.166288	17	Cm242	2.539250E-08	31.289609
18	Np237	3.773680E-01	0.322447	18	Cm242	1.901450E-01	0.430224
102	Pu238	7.009800E-01	0.420251	102	Cm244	6.740970E-01	0.449939
16	Pu238	4.710640E-04	6.12255	16	Cm244	1.335540E-04	5.334437
17	Pu238	7.167710E-06	31.301805	17	Cm244	4.262480E-08	31.293533
18	Pu238	1.157350E+00	0.225476	18	Cm244	4.703140E-01	0.309608
102	Pu239	4.600240E-01	0.389941	102	Cm245	5.011630E-01	0.231848
16	Pu239	4.186680E-04	3.083542	16	Cm245	5.975680E-04	2.98073
17	Pu239	1.001350E-07	31.577203	17	Cm245	1.170420E-07	30.467961
18	Pu239	1.776460E+00	0.213736	18	Cm245	2.654470E+00	0.209694
102	Pu240	4.795250E-01	0.610101	102	Nd143	2.492760E-01	1.255908
16	Pu240	2.478210E-04	5.190497	16	Nd143	8.165080E-04	4.737008
17	Pu240	3.974150E-07	29.398373	107	Nd143	1.376800E-04	0.443999
18	Pu240	4.184660E-01	0.300864	103	Nd143	1.138220E-06	7.186578
102	Pu241	4.136830E-01	0.272259	102	Nd144	6.792360E-02	1.102373
16	Pu241	2.600220E-03	2.350308	16	Nd144	4.365160E-04	7.423914
17	Pu241	4.614380E-06	26.481341	107	Nd144	4.996820E-06	1.085933
18	Pu241	2.429140E+00	0.213053	103	Nd144	3.561940E-07	15.354501
102	Pu242	4.091400E-01	0.396781	102	Nd145	3.979730E-01	0.778601
16	Pu242	6.773920E-04	4.276889	16	Nd145	1.392180E-03	4.003478
17	Pu242	5.481720E-06	28.899649	107	Nd145	2.550110E-05	0.25603
18	Pu242	2.954810E-01	0.338662	103	Nd145	3.022370E-07	12.859423
102	Am241	1.738310E+00	0.236877	102	Nd146	7.997000E-02	0.793858
16	Am241	1.146240E-04	5.500886	16	Nd146	5.630930E-04	6.935479
17	Am241	1.486460E-07	31.37198	107	Nd146	7.484410E-07	3.315108
18	Am241	3.103200E-01	0.373212	103	Nd146	8.417900E-08	21.815338
102	Am242m	4.384440E-01	0.233281	102	Nd148	1.173870E-01	1.188946
16	Am242m	6.080210E-04	3.046048	16	Nd148	6.811340E-04	6.257653
17	Am242m	4.785880E-09	31.08413	107	Nd148	1.112940E-07	9.867565
18	Am242m	3.086350E+00	0.206377	103	Nd148	2.912010E-08	24.447094
102	Am243	1.418950E+00	0.250074	102	Nd150	1.243100E-01	1.3192
16	Am243	3.190080E-04	5.326487	16	Nd150	6.260920E-04	6.482218
17	Am243	6.635170E-07	30.105505	107	Nd150	2.215580E-08	19.409075
18	Am243	2.295710E-01	0.392367	103	Nd150	1.055220E-08	26.166713

Table XXVI: Calculated one-group cross sections for Sample 36 (Pu241)

Reaction (MT)	Isotope	XS [barn]	Relative Error [%]	Reaction	Isotope	XS [barn]	Relative Error [%]
102	Pu238	7.058120E-01	0.442262	102	Nd144	7.023000E-02	1.075616
16	Pu238	6.308990E-04	5.375226	16	Nd144	5.651300E-04	6.238304
17	Pu238	3.917860E-07	41.859071	107	Nd144	5.210990E-06	0.982828
18	Pu238	1.159250E+00	0.229085	103	Nd144	2.847780E-07	9.942706
102	Pu239	4.651190E-01	0.422382	102	Nd145	4.104960E-01	0.812978
16	Pu239	4.727810E-04	3.11634	16	Nd145	1.690620E-03	3.849516
17	Pu239	9.034630E-10	42.562482	107	Nd145	2.575400E-05	0.256518
18	Pu239	1.785230E+00	0.219456	103	Nd145	2.703550E-07	8.196362
102	Pu240	4.775640E-01	0.445268	102	Nd146	8.113920E-02	0.837365
16	Pu240	3.233130E-04	4.652343	16	Nd146	7.396350E-04	5.888609
17	Pu240	6.769620E-08	31.412545	107	Nd146	7.675940E-07	2.150585
18	Pu240	4.190620E-01	0.304106	103	Nd146	4.392080E-08	17.856296
102	Pu241	4.179980E-01	0.291499	102	Nd148	1.154950E-01	1.275674
16	Pu241	2.771410E-03	2.311936	16	Nd148	9.014390E-04	5.435113
17	Pu241	1.960410E-06	30.372155	107	Nd148	9.804800E-08	5.769099
18	Pu241	2.442440E+00	0.217433	103	Nd148	1.089000E-08	21.315547
102	Pu242	4.165960E-01	0.470125	102	Nd150	1.275110E-01	1.552029
16	Pu242	8.598570E-04	4.039659	16	Nd150	8.215580E-04	5.550308
17	Pu242	1.301690E-06	31.659382	107	Nd150	1.247380E-08	13.451382
18	Pu242	2.966560E-01	0.343394	103	Nd150	3.090530E-09	25.958101
102	Nd143	2.568710E-01	1.374745	102	Am241	1.749900E+00	0.239709
16	Nd143	1.007090E-03	4.305101	16	Am241	1.479940E-04	4.847007

107	Nd143	1.406230E-04	0.465366	17	Am241	1.817260E-09	42.329336
103	Nd143	1.185110E-06	4.755913	18	Am241	3.121010E-01	0.377042

Table XXVII: Calculated one-group cross sections for Sample 44 (Am241)

Reaction (MT)	Isotope	XS [barn]	Relative Error [%]	Reaction	Isotope	XS [barn]	Relative Error [%]
102	Pu238	7.15E-01	0.439071	102	Cm242	3.20E-01	0.696929
16	Pu238	6.57E-04	5.943002	16	Cm242	2.38E-05	4.998508
17	Pu238	1.74E-05	41.166286	17	Cm242	7.37E-08	44.721618
18	Pu238	1.16E+00	0.242364	18	Cm242	1.88E-01	0.463897
102	Pu239	4.70E-01	0.421265	102	Nd143	2.73E-01	1.630597
16	Pu239	4.91E-04	3.274646	16	Nd143	1.09E-03	4.978627
17	Pu239	8.10E-07	44.426479	107	Nd143	1.42E-04	0.506585
18	Pu239	1.79E+00	0.228711	103	Nd143	1.72E-06	8.386463
102	Pu240	4.89E-01	0.574415	102	Nd144	6.94E-02	1.136008
16	Pu240	3.37E-04	5.22022	16	Nd144	6.70E-04	7.07982
17	Pu240	1.18E-06	38.432812	107	Nd144	5.31E-06	1.466906
18	Pu240	4.16E-01	0.324099	103	Nd144	7.03E-07	15.547196
102	Pu241	4.24E-01	0.29163	102	Nd145	4.22E-01	0.849087
16	Pu241	2.84E-03	2.429568	16	Nd145	1.75E-03	4.19238
17	Pu241	7.21E-06	21.891545	107	Nd145	2.58E-05	0.29836
18	Pu241	2.46E+00	0.231387	103	Nd145	5.60E-07	13.261051
102	Pu242	4.21E-01	0.470323	102	Nd146	8.26E-02	1.043565
16	Pu242	8.51E-04	4.354633	16	Nd146	8.43E-04	6.608786
17	Pu242	1.07E-05	31.357252	107	Nd146	9.26E-07	4.955922
18	Pu242	2.93E-01	0.364198	103	Nd146	1.91E-07	22.328249
102	Am241	1.78E+00	0.257265	102	Nd148	1.23E-01	1.298961
16	Am241	1.58E-04	5.533504	16	Nd148	9.78E-04	6.053656
17	Am241	8.21E-07	44.176006	107	Nd148	1.80E-07	11.955687
18	Am241	3.07E-01	0.401124	103	Nd148	6.82E-08	26.993302
102	Am242m	4.47E-01	0.255813	102	Nd150	1.31E-01	1.527894
16	Am242m	7.19E-04	3.272096	16	Nd150	9.16E-04	6.29033
17	Am242m	2.21E-08	43.166216	107	Nd150	4.52E-08	20.929057
18	Am242m	3.12E+00	0.224722	103	Nd150	2.93E-08	31.966866
102	Am243	1.45E+00	0.269671	102	Cm243	5.24E-01	0.252231
16	Am243	4.36E-04	5.398964	16	Cm243	4.34E-04	3.349708
17	Am243	1.30E-06	34.131385	17	Cm243	2.19E-07	43.930055
18	Am243	2.27E-01	0.422734	18	Cm243	2.83E+00	0.228035

Table XXVIII: Calculated one-group cross sections for Sample 2 (Nd145)

Reaction (MT)	Isotope	XS [barn]	Relative Error [%]	Reaction	Isotope	XS [barn]	Relative Error [%]
102	Nd142	2.81E-02	1.027431	107	Nd145	2.55E-05	0.3107
16	Nd142	1.03E-04	18.62023	103	Nd145	4.26E-07	13.991792
107	Nd142	2.52E-06	2.2146	102	Nd146	8.33E-02	1.403236
103	Nd142	2.39E-06	5.681982	16	Nd146	7.66E-04	7.042987
102	Nd143	2.49E-01	1.21346	107	Nd146	8.24E-07	4.458915
16	Nd143	1.01E-03	5.283313	103	Nd146	1.34E-07	22.96326
107	Nd143	1.38E-04	0.568592	102	Nd148	1.24E-01	1.632772
103	Nd143	1.44E-06	8.359074	16	Nd148	9.21E-04	6.449066
102	Nd144	6.73E-02	1.268426	107	Nd148	1.43E-07	12.093025
16	Nd144	5.95E-04	7.488501	103	Nd148	4.97E-08	25.582907
107	Nd144	5.09E-06	1.411728	102	Nd150	1.25E-01	1.680664
103	Nd144	5.22E-07	16.542815	16	Nd150	8.48E-04	6.631609
102	Nd145	3.98E-01	0.781678	107	Nd150	3.42E-08	21.540802
16	Nd145	1.66E-03	4.655455	103	Nd150	1.87E-08	27.028609

Table XXIX: Calculated one-group cross sections for Sample 3 (Pd105)

Reaction (MT)	Isotope	XS [barn]	Relative Error [%]	Reaction	Isotope	XS [barn]	Relative Error [%]
102	Pd104	2.19E-01	1.019773	107	Pd106	2.13E-06	1.689971
16	Pd104	9.49E-05	15.164891	103	Pd106	6.22E-06	5.498255
107	Pd104	2.00E-05	0.968657	102	Pd107	9.17E-01	0.420714
103	Pd104	2.03E-05	2.940298	16	Pd107	1.54E-03	5.12932
102	Pd105	8.25E-01	0.433807	107	Pd107	1.24E-06	2.407368

16	Pd105	5.04E-04	7.167139	103	Pd107	1.96E-06	6.959399
107	Pd105	6.99E-06	2.011155	102	Pd108	1.75E-01	1.051305
103	Pd105	1.30E-05	3.870212	16	Pd108	2.30E-04	12.478562
102	Pd106	1.93E-01	1.147274	107	Pd108	5.34E-07	1.517169
16	Pd106	1.61E-04	13.786093	103	Pd108	1.14E-06	9.465782

Table XXX: Calculated one-group cross sections for Sample 4 (Cs133)

Reaction (MT)	Isotope	XS [barn]	Relative Error [%]	Reaction	Isotope	XS [barn]	Relative Error [%]
102	Cs133	4.07E-01	0.721867	107	Cs135	1.19E-07	14.444849
16	Cs133	1.86E-04	14.29447	103	Cs135	3.38E-07	11.73155
107	Cs133	3.95E-07	6.235385	102	Cs136	1.72E-01	0.945671
103	Cs133	3.07E-06	5.614233	16	Cs136	1.41E-03	5.212342
102	Cs134	9.77E-01	0.480507	107	Cs136	1.08E-07	12.979976
16	Cs134	1.24E-03	5.402855	103	Cs136	2.77E-07	10.638784
107	Cs134	2.84E-07	8.740878	102	Cs137	1.50E-02	0.447905
103	Cs134	9.36E-07	6.588188	16	Cs137	4.82E-04	8.890638
102	Cs135	1.97E-01	1.965083	107	Cs137	5.60E-08	17.581152
16	Cs135	3.25E-04	11.303191	103	Cs137	7.76E-08	21.913167

Table XXXI: Calculated one-group cross sections for Sample 5 (Ru101)

Reaction (MT)	Isotope	XS [barn]	Relative Error [%]	Reaction	Isotope	XS [barn]	Relative Error [%]
102	Ru99	5.14E-01	0.613225	102	Ru102	1.46E-01	0.782423
16	Ru99	3.61E-04	8.584078	16	Ru102	7.66E-05	16.121766
107	Ru99	1.87E-04	0.483737	107	Ru102	2.52E-06	1.865327
103	Ru99	4.21E-05	1.767726	103	Ru102	2.02E-07	13.568625
102	Ru101	6.53E-01	0.434622	102	Ru104	1.40E-01	1.162442
16	Ru101	4.51E-04	6.961693	16	Ru104	1.39E-04	13.859536
107	Ru101	3.11E-06	2.072345	107	Ru104	8.13E-08	12.422718
103	Ru101	2.34E-06	6.530199	103	Ru104	1.41E-07	16.977216

Table XXXII: Calculated one-group cross sections for Sample 6 (Mo95)

Reaction (MT)	Isotope	XS [barn]	Relative Error [%]	Reaction	Isotope	XS [barn]	Relative Error [%]
102	Mo92	4.94E-02	1.157715	107	Mo96	9.95E-06	2.335464
16	Mo92	4.09E-07	50.000259	103	Mo96	2.80E-06	6.624573
107	Mo92	1.70E-05	2.50946	102	Mo97	2.98E-01	0.754448
103	Mo92	1.28E-03	1.426761	16	Mo97	5.34E-04	6.395697
102	Mo94	8.64E-02	1.185902	107	Mo97	1.21E-05	1.100379
16	Mo94	5.88E-05	17.924637	103	Mo97	1.73E-06	6.406667
107	Mo94	1.13E-04	1.164978	102	Mo98	1.01E-01	2.340548
103	Mo94	3.76E-05	2.917465	16	Mo98	1.97E-04	11.2447
102	Mo95	2.86E-01	0.696335	107	Mo98	1.02E-06	4.453965
16	Mo95	2.98E-04	8.387237	103	Mo98	1.78E-07	13.404273
107	Mo95	5.42E-05	0.584334	102	Mo100	8.37E-02	2.54908
103	Mo95	6.19E-06	4.243817	16	Mo100	2.51E-04	10.901121
102	Mo96	7.50E-02	1.60566	107	Mo100	1.73E-07	9.722251
16	Mo96	1.16E-04	14.01882	103	Mo100	2.75E-08	20.233978

Table XXXIII: Calculated one-group cross sections for Sample 17 (Sm149)

Reaction (MT)	Isotope	XS [barn]	Relative Error [%]	Reaction	Isotope	XS [barn]	Relative Error [%]
102	Sm144	7.64E-02	0.793889	102	Sm149	1.79E+00	0.442685
16	Sm144	3.05E-05	24.040339	16	Sm149	1.24E-03	4.683788
107	Sm144	1.70E-05	0.850902	107	Sm149	1.78E-05	0.561266
103	Sm144	1.69E-05	1.951226	103	Sm149	4.05E-07	9.543592
102	Sm147	9.64E-01	0.6485	102	Sm150	3.90E-01	0.938065

16	Sm147	6.76E-04	5.981097	16	Sm150	3.84E-04	8.614657
107	Sm147	6.19E-05	0.415246	107	Sm150	4.97E-07	3.769555
103	Sm147	1.56E-06	5.824855	103	Sm150	1.15E-07	18.11555
102	Sm148	2.36E-01	1.132663	102	Sm152	3.67E-01	1.004419
16	Sm148	3.17E-04	9.765922	16	Sm152	3.37E-04	9.702136
107	Sm148	6.80E-06	0.81486	107	Sm152	5.99E-08	11.929181
103	Sm148	1.43E-07	14.382811	103	Sm152	6.65E-08	18.533978

3.4.1 Depletion analysis with MCNP cross sections

The "experimental" axial flux distribution has been provided by the French reports and has been derived by measurements of reaction rates at different places and times. Because of the differences between the experimental and calculated axial flux distributions, a comparison on the Neodymium production for the samples of U235 was performed using the two distributions. There were 6 samples of U235 located along the axis of the core. The results indicated that the experimental distribution provides a consistent (almost constant) set of C/E's, while the calculated one shows a drift in the bottom part. Based on this observation, it was decided that in the analysis we would use the experimental axial distribution. The likely reason for the observed discrepancy has to be attributed to the lack of information on the control rod movement during the cycles, and the actual flux calculations were performed with a fixed average control rod position.

Next step was to correctly normalize the isotope build up results to the actual values of the fluence (and hence eliminate the uncertainty in the irradiation history). To this latter purpose the neodymium production in the U235 samples has been calculated and compared with the correspondent experimental values. The corrective factor, by which the experimental fluxes are divided, has been subsequently derived. The normalization value used in the successive analysis is: **1.047**.

Depletion calculations have been carried out using the NUTS [0] code in order to evaluate the isotope build up. The one group cross sections from the MCNP calculations and normalized fluxes were provided as inputs for the depletion calculations. , The information that can be gathered from the PROFIL post-irradiation analysis is related to the evaluation of the reaction rates (mainly capture and (n,2n) rates) for a given isotope. In particular, the analysis of the experiment is based on the relation existing between the burn-up dependent variations of the atom number densities and the microscopic cross-sections. For isotopes for which the descendant, obtained via neutron capture, is stable or has a long radioactive period, the most accurate experimental technique for obtaining information on the integral capture cross section is to determine the variation in composition that results from high-flux irradiation of a pure sample. Capture and (n,2n) reaction rates for an isotope of mass A, which has received a total fluence of τ, can be evaluated by the measurement of ratios of concentrations using Equations (1) and (2) respectively:

$$\sigma_{(c),A} \cdot \tau \cdot f(\tau) \cong \frac{\Delta N_{A+1}}{N_A} = \frac{N_{A+1}(\tau)}{N_A(\tau)} - \frac{N_{A+1}(0)}{N_A(0)} \qquad (1)$$

$$\sigma_{(n,2n),A} \cdot \tau \cdot f(\tau) \cong \frac{\Delta N_{A-1}}{N_A} = \frac{N_{A-1}(\tau)}{N_A(\tau)} - \frac{N_{A-1}(0)}{N_A(0)} \qquad (2)$$

where $f(\tau)$ is a correcting factor which takes into account the physical phenomena different from capture (or (n,2n) reactions) that the considered isotope A can experience during the irradiation. Because

of its definition f(τ) is a measure of the fertile or fissile properties of a given isotope, being lower and higher than one for fertile and fissile isotopes respectively. It can be evaluated by a time dependent calculation, as follows:

$$f(\tau)=\left[\frac{N_{A+1}^{(\tau)}}{N_A^{(\tau)}}-\frac{N_{A+1}^{(0)}}{N_A^{(0)}}\right]\times\frac{1}{\sigma_{CA}\cdot\tau_{calc.}} \qquad (3)$$

In Equation (3), σ_{CA} and τ_{calc}. represent the one-group capture cross section for the isotope A and the calculated fluence, respectively.

This approach works very well when we are considering a reaction rate that is dominant in the formation of the measured resulting isotope (i. e., capture cross section) but it will attribute the same C/E also when the reaction rate is not dominant like in the case of an (n,2n) cross section. In order to avoid this problem a slightly different approach was adopted. We correct the experimental density variation by a calculated quantity that takes out the variation due to all the phenomena other than the reaction rate that we are considering:

$$\sigma_{(c),A}\cdot\tau\cdot\cong\frac{^{corr}\Delta N_{A+1}}{N_A}=\frac{^{exp}\Delta N_{A+1}(\tau)-(^{calc}\Delta N_{A+1}-N_A^{(0)}e^{-\sigma\tau})}{N_A} \qquad (4)$$

where $^{exp}\Delta N_{A+1}(\tau)$ is the experimental measured density variation, and $^{calc}\Delta N_{A+1}$ is the calculated one.

In the end Eq. 4 was used to derive an initial guess for the unknown experimental cross section and then this latter is computed by changing its value until the final measured experimental densities were matched. Using this new approach C/E's were calculated for the sample isotope build up. In Table XXXIV through Table XLVIII, we show, as an example, some selected C/E's on sample final densities and associated one group cross sections. The depletion decay chain used as branching ratio for the Am241 capture 85% to Am242 (and 15% for Am242m) and 83% to Cm242 and 17% to Pu242 for the β decay of Am242. These values were found to produce the most consistent C/E's.

Table XXXIV C/E's: U235 samples

Samples	U236	U235 σ_c
1	0.944	0.942
10	0.949	0.948
19	0.944	0.943
28	0.950	0.949
37	0.953	0.952
46	0.953	0.952

Table XXXV C/E's: U238 samples

Samples	Pu239	U238 σ_c
12	0.985	0.985
23	0.962	0.962
29	0.969	0.969

Table XXXVI C/E's: Pu238 samples,

Samples	Pu239	Pu238 σ_c
7	1.113	1.299
42	1.112	1.299

Table XXXVII C/E's: Pu239 samples

Samples	Pu238	Pu240	Pu239 σ_c	Pu239 $\sigma_{n,2n}$
9	0.770	0.918	0.918	0.761
20	-	0.901	0.901	-
26	0.6736	0.899	0.899	0.728

Table XXXVIII C/E's: Pu240 samples

Samples	Pu239	Pu241	Pu240 σ_c	Pu241 $\sigma_{n,2n}$
13	0.731	0.956	0.957	0.680
22	0.828	0.960	0.960	0.878
30	-	0.964	0.964	-

Table IXXIX C/E's: Pu241 samples

Samples	Pu242	Pu241 σ_c
35	0.940	0.940
18	0.970	0.956
24	0.970	0.955

Table XL C/E's: Pu242 sample

Samples	Am243	Cm244	Pu242 σ_c	Am243 σ_c
15	1.058	0.826	1.058	0.768
32	1.044	0.933	1.045	0.890
40	1.078	0.925	1.079	0.852

Table XLI C/E's: Am241 samples

Samples	Pu238	Pu242	Am242	[a)]Am241 σ_c	[b)]Am241 σ_c	[c)]Am241 σ_c
11	0.949	0.965	0.972	0.969	0.965	0.944
44	0.949	0.988	1.001	1.001	0.988	0.945

a) Calculated from Am242 build up. b) Calculated from Pu242 build up. c) Calculated from Pu238 build up

Table XLII C/E's: Mo95

Samples	Mo96	Mo95 σ_c
6	1.042	1.067
33	0.997	0.996

Table XLIII C/E's: Mo97 samples

Samples	Mo98	Mo97 σ_c
6	0.981	0.956
33	1.008	0.980

Table XLIV C/E's: Ru101 samples

Samples	Ru102	Ru101 σ_c
5	1.076	1.094
27	1.093	1.112
39	1.079	1.097

Table XLV C/E's: Pd105 samples

Samples	Pd106	Pd105 σ_c
3	0.894	0.858
34	0.878	0.845

Table XLVI C/E's: Cs133 samples

Samples	Cs134	Cs133 σ_c
4	0.868	0.868
31	0.890	0.890

Table XLVIIC/E's: Nd145 samples

Samples	Nd146	Nd145 σ_c
2	0.983	0.961
41	0.974	0.948

Table XLVIII C/E's: Sm149 samples

Samples	Sm150	Sm149 σ_c
17	0.922	0.925
45	0.878	0.905

3.4.2 Depletion analysis with deterministic methodology

In the following we report details of the deterministic calculation methodology used for the PROFIL-1 analysis including multi-group cross section generation at the lattice cell level, full core burn-up, irradiation pin data extraction and condensation, and fine irradiation of isotope samples.
All neutronics calculations have been performed with modules of the ERANOS 2.1 code system. The cross sections with original data derived from the ENDF/B-VII evaluation have been processed over a 33-group energy structure with the ECCO code. The spatial flux was obtained via the 3D VARIANT code based on the variational nodal transport method in P_3 approximation and HEX-Z geometry. Fine irradiation and cooling of the isotope samples was performed with the MECCYCO fuel cycle code.

To prepare 33-group cross sections for the full core burn-up calculation, every material region in each PHENIX subassembly type was represented by an 2D ECCO unit cell. The active fuel regions of the three fuel subassembly types were modeled as heterogeneous cells with 217 fuel pins in a hexagonal lattice. Fuel pins, gap, clad, and wrapper tube were explicitly represented in accordance with geometrical data for PHENIX fuel subassemblies. The fuel pin spacer wire was smeared into the interstitial sodium coolant. All other material regions such as the axial and radial blankets, reflectors, and plenum were modeled as homogeneous regions with all number densities smeared into a hexagon. Number densities for all cells were derived from a R-Z PHENIX model provided by a French report [11]. Nuclide mass was preserved when converting the R-Z region volumes and number densities into HEX-Z geometry.

The ECCO "reference route" presented in the ERANOS documentation was used to produce subassembly-averaged cross sections. For the heterogeneous fuel cells, collision probabilities are used for the flux solution and resonance self-shielding while the fundamental mode is assumed for homogenous cells. Heavy isotopes and common structural isotopes are treated at the fine group level (1968 energy group library) and cross sections are condensed to the 33-group structure. Fission product cross sections are originally derived from a 33 energy group library. Figure 11 shows the ECCO calculation steps used for the PROFIL-I analysis.

Figure 11: ECCO Reference route steps for heterogeneous fuel unit cells.

ECCO Reference Route

```
>STEP_1_FUEL_HET
   GEOMETRY HOMOGENEOUS
   GROUP STRUCTURE OTHER 33
   INPUT LIBRARY 'ENDF_33
   ELEMENTS ALL
   FLUX SOLUTION FM P1 CONSISTENT ORDER 1
   BSEARCH 1.0
   SELF SHIELDING NODBBSH ;
->STEP_2_FUEL_HET
    GEOMETRY ORIGINAL
    GROUP STRUCTURE OTHER 33
    INPUT LIBRARY 'ENDF_33'
    ELEMENTS ALL
    FLUX SOLUTION CP P1 CONSISTENT ORDER 1
    BFROM 1
    LEAKAGE NLFACT CELL BENOIST FLUXWT MEAN
    SELF SHIELDING NODBBSH ;
->STEP_3_FUEL_HET
   GEOMETRY ORIGINAL
   GROUP STRUCTURE FINE
    INPUT LIBRARY 'ENDF_1968'
    ELEMENTS 42
      'Na23' 'Fe54' 'Fe56  'Fe57' 'Fe58' 'Cr50  'Cr52'
      'Cr53' 'Cr54' 'Ni58'  'Ni60' 'Ni61' 'Ni62' 'Ni64'
      'Mo92' 'Mo94  'Mo95' 'Mo96' 'Mo97' 'Mo98'
      'Mo100' 'U235' 'U238' 'Pu239' 'Pu240' 'Pu241'
      'Pu242' 'Mn55' 'Si28' 'Si29' 'Si30' 'Pu238' 'Np237'
      'Np239' 'Am241' 'Am242m' 'Am243' 'Cm242'
      'Cm243' 'Cm244' 'Cm245' 'O16'

! Step 3 continued
 FLUX SOLUTION CP P1 CONSISTENT ORDER 1
    BFROM 1
   LEAKAGE NLFACT CELL BENOIST FLUXWT MEAN
   SELF SHIELDING NODBBSH
    CONDENSE 33
        1 82 142 202 262 322 382 442 502 564 624
        686 746 808 868 928 988 1048 1108 1168
        1228 1288 1336 1422 1480 1516 1579 1648 1708
        1768 1837 1919 1952  ;
->STEP_4_FUEL_HET
    GEOMETRY ORIGINAL
    GROUP STRUCTURE OTHER 33
    FLUX SOLUTION CP P1 CONSISTENT ORDER 1
    BSEARCH 1.0
    LEAKAGE NLFACT CELL BENOIST FLUXWT MEAN ;
 >STEP_5_FUEL_HET
    HOMOGENISE
    GEOMETRY HOMOGENEOUS
    GROUP STRUCTURE OTHER 33
    FLUX SOLUTION FM P1 CONSISTENT ORDER 1
    BFROM 4
    ! LEAKAGE NFLACT CELL BENOIST FLUXWT MEAN
    PRINT DATA FLUXES
    CROSS SECTIONS MICROSCOPIC VECTORS ;
```

A modified ECCO calculation was performed for the center fuel subassembly which contains the irradiation pin in the third ring as shown in Figure 12. The ROTH x 6 surface method was used in the calculation route instead of the default collision probability option. The largest effect of the collision probability method was on the capture cross section of U238. For each actinide isotope sample type (U235, U238, Pu238, Pu239, Pu240, Pu241, Pu242, and Am241), a separate ECCO calculation was run with the mass of the corresponding oxide sample smeared in the interior volume of the sample capsule represented in the irradiation pin of the cell model. For the fission product samples, a single ECCO calculation was run with the capsule filled with equal fractions of each type of fission product sample.

Figure 12: Central PHENIX Subassembly containing 217 fuel pins with a third ring pin replaced with the PROFIL-I irradiation pin modeled with the general lattice ECCO option.

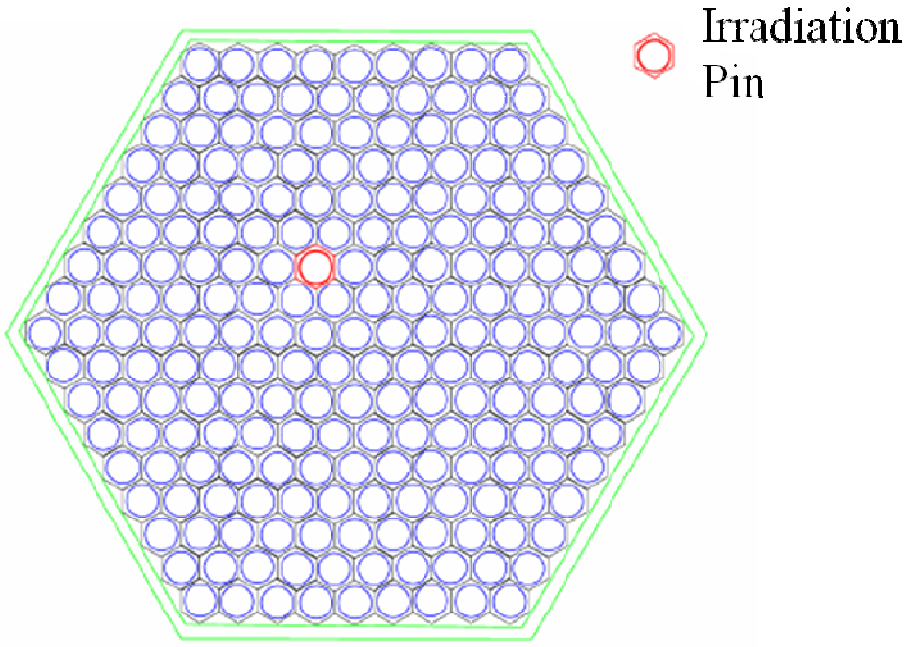

The first three irradiation cycles of PHENIX were modeled with a full core burn-up calculation with VARIANT providing the 33-group flux solution. The fuel regions were subdivided into 5 axial regions and the axial blankets were modeled as single zones. The actinide chains were explicitly tracked while Mo99 was used as the characteristic fission product. An average control rod position was used over all three cycles. At the beginning of each irradiation cycle, cross sections were recalculated in the burnable zones using the nuclide concentrations at the corresponding time. Figure 13 shows the calculated cycle dependent axial flux profile normalized to the "experimental" flux along the irradiation pin. Figure 14 shows the 33-group flux spectrum at the core midplane for Cycle 1.

Figure 13: Burn-up dependent axial flux profiles along the irradiation pin. Z = 0 corresponds to Sample 19 at the core midplane.

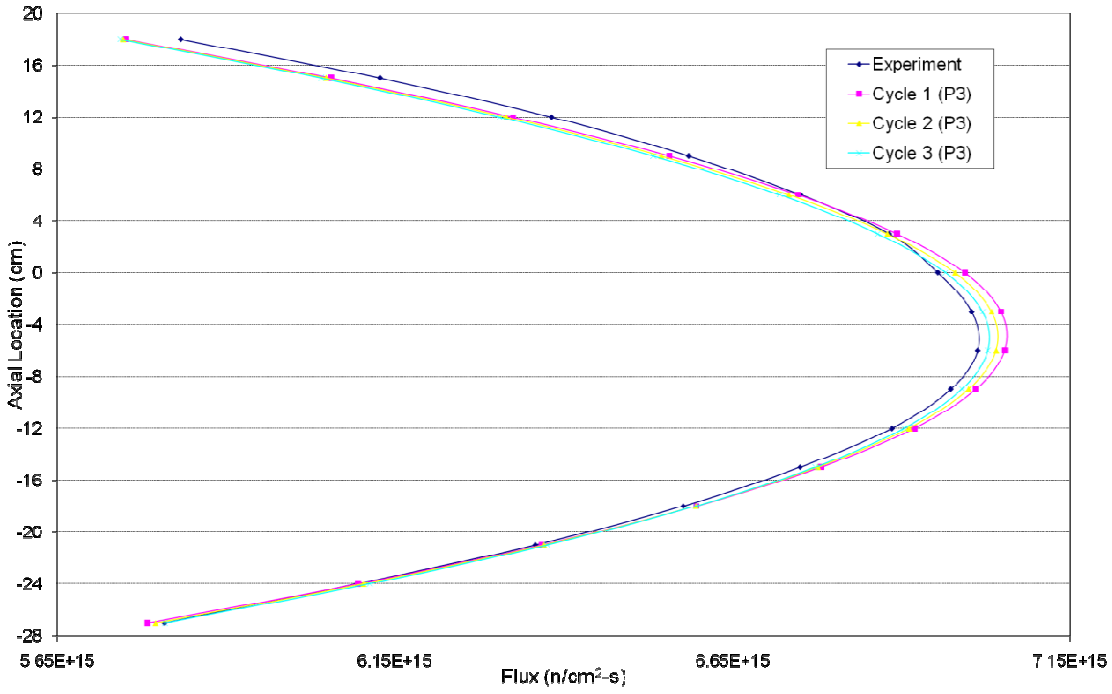

Figure 14: Cycle and axial position dependent flux spectra used as weighting function for one energy-group cross section generation for isotope samples.

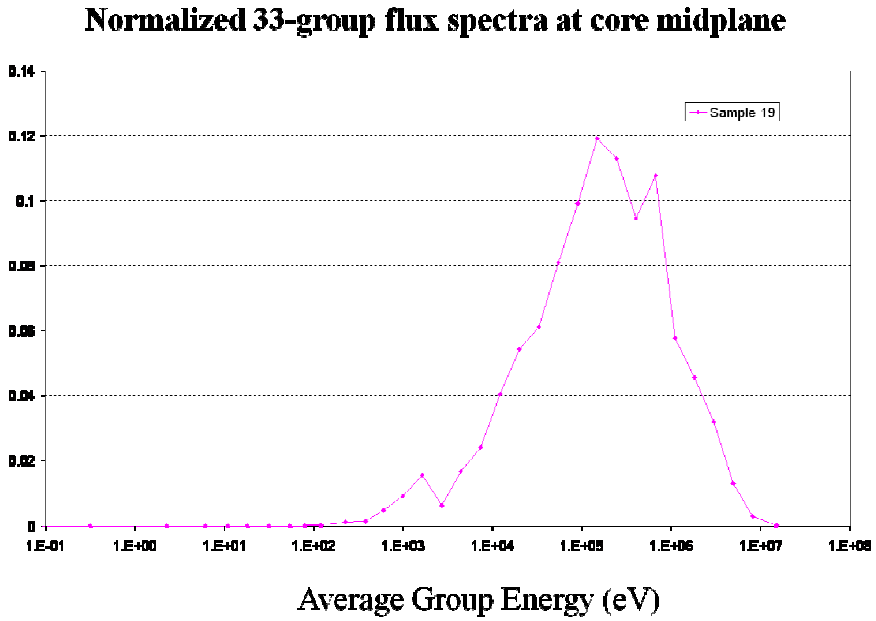

The ECCO model for the center subassembly provides 33-group cross sections for each sample type. The cycle dependent flux solutions provide 33-group flux spectra along the vertical axis of the irradiation pin.

LU (ERANOS User's Language) procedures were developed to directly access and extract the (n,f), (n,2n), and (n,γ) 33-group cross sections for isotopes of the sample from the MICRO EDL (EDLs are data sets produced, stored , and accessed by ERANOS modules). Another LU procedure extracts the 33-group flux spectra at each sample axial location and burn-up cycle from the ASVL EDL. Finally, the extracted flux spectra are used as weighting functions to collapse the cross sections to one energy-group to obtain cycle dependent, locally flux-weighted cross sections for every sample.

A detailed burn-up calculation for each sample was performed by the MECCYCO fuel cycle code. The one energy-group cross sections and initial isotope concentrations were provided as inputs to MECCYCO. The "experimental" flux profile and six-step burn-up scheme (3 irradiation steps and 3 cooling periods) that have been described in previous reports were utilized. Fission yields for the Nd isotopes were obtained from ENDF/B-VII evaluation through the JANIS 3.2 nuclear information software.

Nuclear decay data is provided in a library reference file that comes with the ERANOS cross section library files. Either a processing error by a MECCYCO/ERANOS function or erroneous data in the ENDF/B-VII reference file resulted in the decay constant for ground state Am242 to be set to zero indicating a stable isotope. The decay constant for ground state Am242 stored in the DECAY CHAIN EDL created by the MECCYCO/ERANOS function CREATION_CHAINE_EVOLUTION had to be manually changed to the correct decay constant value of 1.201878E-5 s^{-1}. Some decay data such as branching ratios have to be provided by the user. The branching values for capture on Am241 were set to 85%/15% to ground state Am242 and metastable Am242, respectively. The branching values for the decay of ground state Am242 were set to 83%/17% for beta- decay to Cm242 and electron capture to Pu242, respectively.

Six U235 samples were dispersed axially in the PROFIL-I irradiation pin. These samples serve as fluence monitors. The actual fluence can be derived by measuring the ratios of fission products with small absorption cross sections and well known fission yields (such as Nd) to U235. The C/E values for Nd concentrations in the U235 samples are shown in Table XLIX. For Nd143, Nd145, Nd146, and Nd148, the experimental flux was divided by a fluence normalization factor to obtain an average C/E equal to 1 over all U235 samples (except for Sample 19). An average fluence normalization factor of **1.045** was obtained by averaging together the factors obtained for each individual Nd isotope.

U235 Samples Before Fluence Normalization							
	Sample 1	Sample 10	Sample 19	Sample 28	Sample 37	Sample 46	Average
'U234'	1.012	1.013	1.014	1.014	1.009	1.007	1.011
'U236'	1.007	1.003	0.997	1.002	1.004	1.011	1.004
'U238'	1.006	1.001	0.994	1.013	1.015	0.990	1.003
'Nd143'	1.041	1.042	1.048	1.040	1.041	1.041	1.042
'Nd144'	1.071	1.068	1.210	1.102	1.075	1.064	1.098
'Nd145'	1.044	1.041	1.050	1.037	1.041	1.041	1.042
'Nd146'	1.061	1.056	1.066	1.050	1.045	1.040	1.053
'Nd148'	1.072	1.072	1.072	1.063	1.066	1.064	1.068
'Nd150'	1.094	1.092	1.097	1.087	1.087	1.086	1.090

Table XLIX: C/E values for U235 samples before fluence normalization. Neodymium production from fission and Uranium isotope buildup

U235 Samples After Fluence Normalization							
	Sample 1	Sample 10	Sample 19	Sample 28	Sample 37	Sample 46	Average
'U234'	1.005	1.006	1.006	1.006	1.001	1.001	1.004
'U236'	0.962	0.958	0.952	0.957	0.959	0.966	0.959
'U238'	0.999	0.993	0.985	1.004	1.006	0.982	0.995
'Nd143'	0.992	0.992	0.998	0.990	0.991	0.992	0.993
'Nd144'	1.019	1.016	1.150	1.048	1.022	1.013	1.045
'Nd145'	0.995	0.992	1.000	0.987	0.991	0.992	0.993
'Nd146'	1.010	1.004	1.013	0.998	0.993	0.990	1.001
'Nd148'	1.021	1.021	1.020	1.012	1.014	1.013	1.017
'Nd150'	1.042	1.040	1.044	1.035	1.035	1.035	1.038

Table L: **C/E values for U235 samples after fluence normalization.**

Tables LI to LXIV show the C/E values for all isotope concentrations in the PROFIL-I samples. These values have been calculated using the six-step burn-up scheme adjusted by the fluence normalization factor.

Table LI: C/E U238 Samples.

	Sample 12	Sample 23	Sample 29
'U235'	0.995	0.996	0.985
'Pu239'	0.970	0.967	0.964
'Pu240'	0.939	0.934	0.932
'Pu241'	0.961	1.000	0.989

Table LII: C/E Pu238 Samples.

	Sample 7	Sample 42
'Pu239'	1.130	1.123
'Pu240'	1.024	1.021
'Pu241'	1.018	1.013
'Pu242'	0.997	0.982

Table LIII: C/E Pu239 Samples.

	Sample 9	Sample 20	Sample 26
'Pu238'	0.704	0.000	0.649
'Pu240'	0.928	0.918	0.923
'Pu241'	0.908	0.876	0.900
'Pu242'	1.273	0.000	1.431

Table LIV: C/E Pu240 Samples.

	Sample 13	Sample 22	Sample 30
'Pu238'	0.779	0.907	0.805
'Pu239'	0.704	0.786	0.362
'Pu241'	0.972	0.976	0.979
'Pu242'	1.004	0.962	0.993

Table LV: C/E Pu241 Samples.

	Sample 18	Sample 24	Sample 35
'Pu238'	0.502	0.501	1.950
'Pu239'	0.995	0.995	1.686
'Pu240'	1.000	0.999	1.102
'Pu242'	0.964	0.965	0.984

Table LVI: C/E Pu242 Samples.

	Sample 15	Sample 32	Sample 40
'Pu238'	0.744	0.871	0.944
'Pu239'	1.007	0.995	1.076
'Pu240'	1.004	1.000	1.004
'Pu241'	1.009	1.015	1.005
'Am242m'	3.055	2.479	3.042
'Am243'	1.071	1.045	1.071
'Cm242'	2.804	2.873	2.880
'Cm244'	0.839	0.934	0.920

Table LVII: C/E Cs133 Samples.

	Sample 4	Sample 31
'Cs134'	0.908	0.899
'Cs135'	1.595	1.578

Table LVIII: C/E Am241 Samples.

	Sample 11	Sample 44
'Am242m'	0.971	1.000
'Am243'	0.998	0.810
'Pu238'	0.971	0.968
'Pu239'	0.320	0.409
'Pu240'	0.087	0.170
'Pu241'	0.011	0.014
'Pu242'	0.945	0.966
'Cm242'	1.021	1.026

Table LIX: C/E Nd145 Samples.

	Sample 2	Sample 41
'Nd142'	0.995	1.001
'Nd143'	1.000	1.000
'Nd144'	0.998	1.001
'Nd146'	1.009	1.011
'Nd148'	0.994	0.993
'Nd150'	1.017	1.012

Table LX: C/E Pd105 Samples.

	Sample 3	Sample 34
'Pd104'	0.823	0.798
'Pd106'	0.884	0.876
'Pd107'	0.708	0.713
'Pd108'	0.708	0.734

Table LXI: C/E Ru101 Samples.

	Sample 5	Sample 27	Sample 39
'Ru99'	1.013	1.015	1.014
'Ru102'	1.102	1.102	1.103
'Ru104'	1.000	0.919	0.915

Table LXII: C/E Sm149 Samples.

	Sample 17	Sample 45
'Sm144'	0.941	0.951
'Sm147'	0.994	0.997
'Sm148'	0.982	0.985
'Sm150'	0.918	0.924
'Sm151'	0.818	0.830
'Sm152'	0.995	0.997

Table LXIII: C/E Mo95 Samples.

	Sample 6	Sample 33
'Mo97'	1.003	0.893
'Mo92'	0.991	0.796
'Mo94'	0.999	0.931
'Mo96'	1.027	1.004
'Mo98'	0.987	0.819
'Mo100'	0.965	0.751

Table LXIV: C/E Mo97 Samples.

	Sample 8	Sample 43
'Mo92'	0.736	0.913
'Mo94'	0.806	0.941
'Mo95'	0.818	0.937
'Mo96'	0.923	0.971
'Mo98'	0.988	1.008
'Mo100'	0.797	0.914

3.4.3 Summary on PROFIL-1 analysis

Table LXV summarizes the C/E with the ENDF/B-VII one group cross sections obtained using both stochastic and deterministic methodology. These results have been obtained by averaging the corresponding C/Es over the different samples.

We will observe that there is a good consistency between the results obtained with the stochastic methodology and those obtained with the deterministic one as the discrepancies are inside the experimental uncertainties.

Large discrepancies of ENDF/B-VII data are noticeable for capture cross sections of Pu isotopes (Pu238, Pu239, and Pu242) and Am243. The (n,2n) cross sections of Pu239 and Pu240 appear to be largely underestimated. Regarding fission products, the capture cross sections of Ru101, Pd105, Cs133 , and Sm149 need to be improved.

σ	C/E		
	MCNP	Deter.	Exp. Unc.
σ_{capt} U-235	0.948	0.958	1.7 %
σ_{capt} U-238	0.972	0.967	2.3 %
σ_{capt} Pu-238	1.299	1.348	4.0 %
σ_{capt} Pu-239	0.906	0.922	3.0 %
$\sigma_{n,2n}$ Pu-239	0.745	-	15.0 %
σ_{capt} Pu-240	0.964	0.976	2.2 %
$\sigma_{n,2n}$ Pu-240	0.779	-	15.0 %
σ_{capt} Pu-241	0.950	0.956	4.1 %
σ_{capt} Pu-242	1.061	1.062	3.5 %
σ_{capt} Am-241	0.968	-	1.7 %
σ_{capt} Am-243	0.834	-	5.0 %
σ_{capt} Mo-95	1.032	1.025	3.8 %
σ_{capt} Mo-97	0.968	0.993	4.4 %
σ_{capt} Ru-101	1.101	1.124	3.6 %
σ_{capt} Pd-105	0.852	0.834	4.0 %
σ_{capt} Cs-133	0.878	0.905	4.7 %
σ_{capt} Nd-145	0.955	-	3.8 %
σ_{capt} Sm-149	0.915	0.924	3.1 %

Table LXV. Sample averaged C/E for individual cross sections obtained with stochastic (MCNP) and deterministic methodology.

3.5 PROFIL-2 and TRAPU Modeling

Other experiments performed in the PHENIX reactor are PROFIL-2 and TRAPU [9]. In the last fiscal year, PROFIL-2 has been modeled using MCNP calculations (Figure 15). It has two irradiated fuel pins, in which each one has 42 irradiated samples. In order to calculate one-group cross sections for each sample, it is necessary to perform a similar technique to the one shown in Figure 10. In this fiscal year, we have modeled TRAPU for MCNP calculations (Figure 16). In the third assembly ring there are two

subassemblies having total of 10 irradiated fuel pins (5 each). Unlike other two experiments, each irradiated fuel pin has only one sample which has the same size as that of ordinal fuel pin. The large volume of irradiated samples makes Monte Carlo calculations much simpler since the tallies of reactions can be easily done without performing the complicated procedure as shown in Figure 10. In the next fiscal year, we will perform depletion calculations and finalize the analysis of both PROFIL-2 and TRAPU.

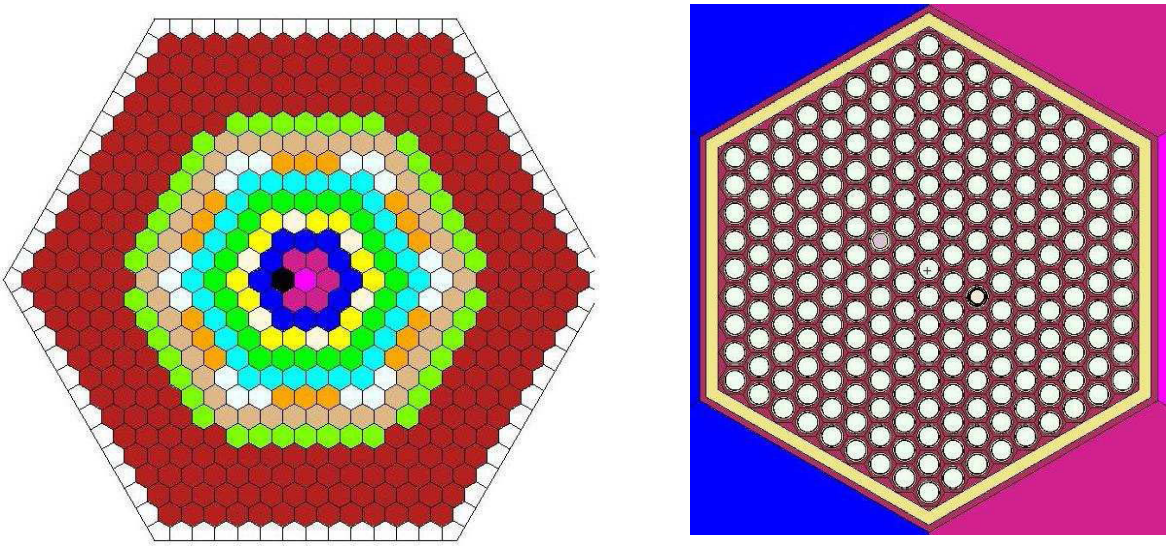

(a) Radial configuration during PROFIL-2 experiment (b) Subassembly containing irradiated samples

Figure 15: Radial cross sectional view of the PROFIL-2 model by MCNP5.

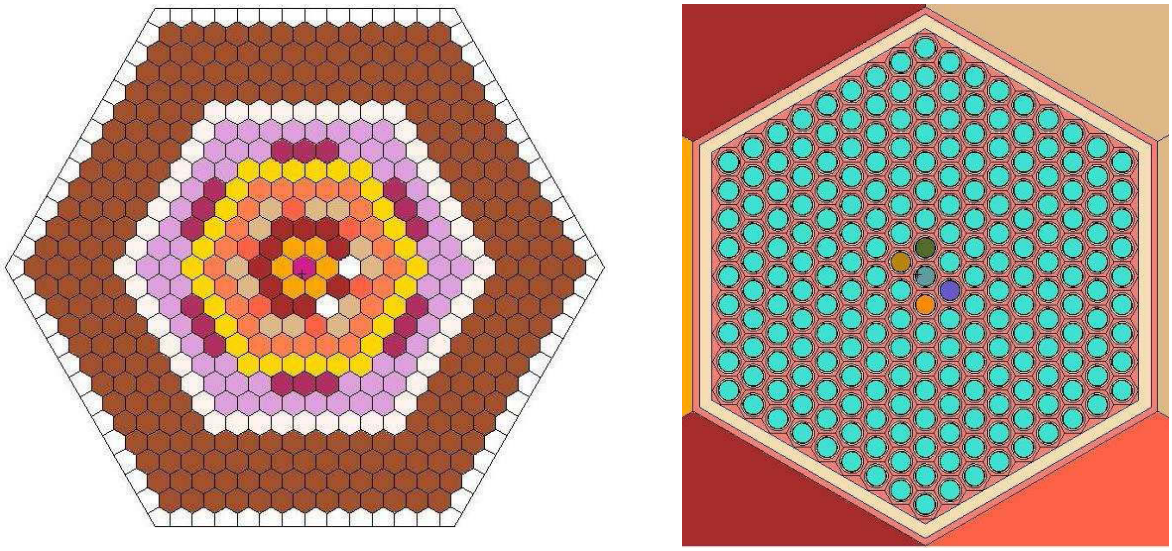

(a) Radial configuration during TRAPU experiment (b) Subassembly containing irradiated samples

Figure 16: Radial cross sectional view of the TRAPU model by MCNP5.

4. CONCLUSIONS

This report has presented the status of activities performed at INL under the AFCI Work Package on "Uncertainty Reduction Analyses" that has a main goal the reduction of uncertainties associated with nuclear data on neutronic integral parameters of interest for the design of advanced fast reactors under consideration by the FCR&D program.

First an analysis of uncertainty evaluation has been presented using the new covariance data (AFCI version 1.2) made available by BNL. The results of the study indicate that a careful analysis is still needed in order to define the most appropriate and effective strategy for data uncertainty reduction. It seems that, besides a further consolidation of the present covariance data libraries, a strategy of combined use of integral and differential measurements should be further pursued in order to meet future requirements.

Subsequent analyses of a number of experiments, among those selected in the previous fiscal year and available, are presented making use of ENDF/B-VII data. These experiments include: updating of the ZPR-6/7 assembly (improved model and spectral indices), ZPPR-9 assembly (only simplified model available), ZPPR-10 (full detailed model), and irradiation experiments including PROFIL-1 detailed analysis and modeling of the PROFIL-2 and TRAPU experiments.

The analysis of the ZPR and ZPPR configurations have indicated a good performance of the ENDF/B cross section data for the core criticality, most of the spectral indices and some reactivity coefficients.

The analysis of the irradiation experiment PROFIL-1 has shown large discrepancies of ENDF/B-VII data for capture cross sections of Pu isotopes (Pu238, Pu239, and Pu242) and Am243. The (n,2n) cross sections of Pu239 and Pu240 appear to be largely underestimated. Regarding fission products, the capture cross sections of Ru101, Pd105, Cs133 , and Sm149 need to be improved.

Because the detailed information of some experiments (in particular ZPPR-9 and ZPPR-15) were not available as well the more reliable covariance data (AFCI version 2.0) it was decided to postpone the planned adjustment. These data should be available next fiscal year. Therefore, for yhe next fiscal year the work to be performed at INL under the support of this Work Package will focus on two main activities:

- Complete analysis for the remaining list of experiments (including ZPPR-9 and ZPPR-15 when available) and finalize irradiation experiment analysis, that at this moment have been only partially analyzed" with ENDF/B-VII data (In particular PROFIL-2 and TRAPU)
- Perform a full multigroup adjustment in the energy structure (33 groups) that has been agreed for design calculations.

For this latter task, the improved covariance matrix AFCI 2.0 is expected to be used.

5. REFERENCES

[1] "OECD/NEA WPEC Subgroup 26 Final Report: Uncertainty and Target Accuracy Assessment for Innovative Systems Using Recent Covariance Data Evaluations", 2008

[2] G. Rimpault et al., "The ERANOS Code and Data System for Fast Reactor Neutronics Analyses", Proc. PHYSOR 2002 Conference, Seoul (Korea), October 2002.

[3] D. Rochman, M. Herman, P. Oblozinsky and. S. F. Mughabghab, "Preliminary Cross-Section Covariances for WPEC Subgroup 26," Tech. Rep. BNL-77407-2007-IR, Brookhaven National Laboratory, 2007

[4] P.Oblozinsky, C.M. Mattoon, M. Herman, S.F. Mughabghab, M.T. Pigni National Nuclear Data Center, (BNL), P. Talou, G.M. Hale, A.C. Kahler, T. Kawano, R.C. Little, P.G. Young, LANL, Los Alamos, "Progress on Nuclear Data Covariances: AFCI-1.2 Covariance Library" September 28, 2009**.**

[5] G. Palmiotti, M. Salvatores, G. Aliberti, H. Hiruta, R. McKnight, P. Oblozinsky, and W.S. Yang, "A global approach to the physics validation of simulation codes for future nuclear systems", Annals of Nuclear Energy **36** (2009) 355–361.

[6] X-5 Monte Carlo Team, "MCNP – A General Monte Carlo N-Particle Transport Code, Version 5," LA-UR-03-1987, Los Alamos National Laboratory (2003).

[7] International Handbook of Evaluated Reactor Physics Benchmark Experiments, NEA/NSC/DOC(2006)1, OECD-NEA, March (2008)

[8] International Handbook of Evaluated Criticality Safety Benchmark Experiments, NEA/NSC/DOC(95)03, September 2008 Edition.

[9] G. Palmiotti, M. Salvatores, and R. N. Hill, "Sensitivity, Uncertainty Assessment, and Target Accuracies Related to Radiotoxicity Evaluation", Nucl. Sci. Eng. **117**, 239 (1994)

[10] J. Tommasi, E. Dupont, and P. Marimbeau, "Analysis of Sample Irradiation Experiments in Phenix for JEFF-3.0 Nuclear Data Validation," Nucl. Sci. Eng., 154, 119-133 (2006).

[11] M. Carnoy, "Donnees necessaries au calcul neutronique du Coeur de Phenix au cours du 1st cycle de fonctionnement", 2NT DRNR/SEDC/SPNR, 77-143.